The analysis, design, and implementation of uplink/downlink antennas for AMSAT AO-40

Wei Bo Sun

A Thesis
in
The Department
of
Electrical and Computer Engineering

Presented in Partial Fulfillment of the Requirements
For the Degree of Master of Applied Science in Electrical Engineering at
Concordia University
Montreal, Quebec, Canada

June 2004

Your file Votre référence
ISBN: 0-612-94710-6
Our file Notre référence
ISBN: 0-612-94710-6

Abstract

The analysis, design, and implementation of
uplink/downlink antennas for AMSAT AO-40

Wei Bo Sun

The antenna is an important component in a radio communication system. Two kinds of antennas, transmitting and receiving antennas, are designed for use in a radio amateur satellite communication system. This thesis introduces the basic theory about antennas, the numerical technique Method of Moments, and wire grid models. It gives the design process for the downlink and uplink antennas, which are used for the satellite communication system. It implements a 2.4 GHz reflector antenna with a helix feed to realize the downlink, and a 435 MHZ 13 turns helix antenna for uplink. It also gives the measured total performance, and provides the computer simulation model.

Acknowledgements

I would like to thank my advisor, Dr. Robert Paknys, for all of his advice and motivation throughout the completion of this thesis. His technical knowledge was an invaluable asset, but maybe more importantly, he helped to keep me focused and pointed in the right direction.

Also, I would like to thank Dr. Christopher W. Trueman, for providing useful software and advice for me.

Table of Contents

List of Figures

List of Tables

Chapter 1

Introduction

A new period for communication began after the first satellite was launched by the USSR in 1957. The first amateur satellite which was developed by radio amateurs was launched by the USA in 1961. Since then, more and more radio amateurs have become interested in satellite communication.

Before the 1980's, these satellites were capable of simple transmit/receive(T/R) experiments. After that, the amateur satellite grogram grew rapidly. This brought more complex equipment like digital transponders and more transmitter power, so we could receive the signal from the satellite easily. The disadvantage of these satellites is that the flight orbit period is short, so one must hurry to operate it in each period.

The largest, most complex and most powerful satellite for the amateur satellite service which is called AO-40 was launched in November, 2000. It has a highly stable elliptical orbit with low inclination. This means that it has very long periods of visibility, at substantial distances (up to 60,000 km). Thus half of the global radio amateurs can communicate with AO-40 at he same time when it is at its apogee. It has a 2.4 GHz and 24 GHz downlink, 70cm and 2m uplink, a digital camera and GPS equipment[1]. The radio amateur satellite corporation (AMSAT) intends to launch another high earth orbit (HEO) P3E satellite in 12 months; it will likely attract more and more amateurs into

satellite communication.

The basic background for radio amateur satellite communication is available in [2]. Currently, the easiest operating mode for of AO-40 is the downlink at 2.4 GHz and uplink at 435 MHz (70cm). Figure1.1 shows the typical T/R system.

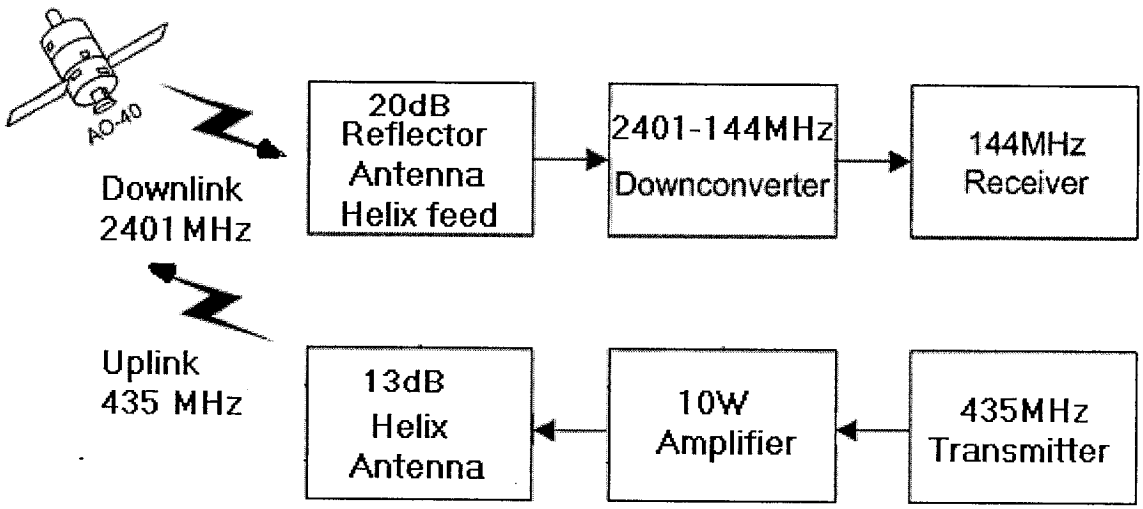

Figure 1.1 Downlink and uplink system of AO-40.

To realize the satellite communication system, we need to have a ground station. Then we should know how to track the satellite position and find the availability time. This is done with orbit-predicting software that can be run on a PC.

The antenna is an important part in the communication system. It receives the electromagnetic wave from the satellite or transmits the electromagnetic wave to the satellite. The performance of the antenna is a major factor in the system performance. So the major task in this thesis is to design the antennas for this satellite system. The popular

types of antennas used by radio amateurs are the dipole, Yagi, helix, parabolic dish, horn, etc. An important characteristic of the antenna used for satellite communication is mostly circular polarization. Polarization is a term to describe direction of the electrical field vector and this will discuss in Chapter 2. All the antennas used on AO-40 are right hand circular polarization (RHCP). For the 2.4 GHz downlink and the 435 MHz uplink, the recommended gain of each antenna is 20 dB and 13 dB respectively. For the UHF uplink, the Yagi antenna is a popular kind of antenna for radio amateur use, but the major disadvantage for this is that most satellites use circular polarization. Howard Long used a pair of orthogonal 8 element Yagis to obtain 12.6 dB gain, using a power splitter[3]. On the other hand, a helix antenna can realize RHCP easily. Long used a quad helix array for a 2.4 GHz downlink[4]. This is also a good choice, but it needs an extra 4 port power splitter. A reflector antenna is a popular choice in the microwave band, because many radio amateurs can easily obtain an old TV satellite dish at low cost. In this thesis, an offset reflector with helix feed was designed and built, for the 2.4 GHz downlink, and a 13 turn helix antenna for the uplink.

Chapter 2 discusses the necessary antenna theory and modeling techniques. We talk about the basic antenna parameters and antenna measurement methods. Chapter 3 discusses the specific design of the downlink antenna, gives the measurement results, and compares experimental results with the computer simulation results. It also describes how to realize the downlink communication with AO-40 and gives the decoded satellite telemetry. Chapter 4 describes the uplink helix antenna. It implements the full size

antenna, measures the parameter and gives the computer simulation result. Chapter 5 contains the conclusions. The purpose of this thesis is to realize the communication with AO-40 at S band and UHF band, establish the earth station with reasonable cost, and to give an introduction to other amateurs who wish to realize this type of system.

Chapter 2

Theory of Antenna and Modeling

2.1 Basic Parameters of Antenna

We begin by describing the basic parameters used to characterize an antenna. They are used for assessing the communication system feasibility and performance. Much of the necessary material for this chapter has been condensed from [5]-[6].

2.1.1 Radiation Pattern

The radiation pattern is a graphical representation of the far field radiation properties of an antenna. Usually, we use two orthogonal principal planes to plot the radiation pattern. These are the E-plane and H-plane.

We also use a normalized field pattern amplitude function $F(\theta,\varphi)$ to indicate the pattern of antenna. If the field is θ–polarized then

$$F(\theta,\varphi)=\frac{E_\theta(\theta,\varphi)}{E_\theta(\max)}. \tag{2-1}$$

In practice, we use the power pattern $P(\theta,\varphi)$ to describe the radiation pattern of the antenna. The power pattern gives the power density angular dependence and is found

from the (θ,φ) variation of the r-component of the Poynting vector. Frequently, the power pattern contains many lobes. The lobe which contains the maximum radiation direction is main lobe. Others are called the minor lobes or side lobes. The power and amplitude patterns are related by

$$P(\theta,\varphi) = |F(\theta,\varphi)|^2 . \tag{2-2}$$

HPBW is the half power beamwidth, which is the angular separation of the points where the main beam of the power pattern equals 1/2 of its maximum value.

FNBW is the first null power beamwidth, which is the angular separation of the points where the main beam of the power equals 0.

2.1.2 Directivity D and Gain G

Directivity is the ratio of the radiation of the maximum intensity $U(\theta,\varphi)_{\max}$ in a certain direction to the average radiation intensity U_{ave}.

$$D = \frac{U(\theta,\varphi)_{\max}}{U_{ave}} = \frac{4\pi U(\theta,\varphi)_{\max}}{P_{rad}} = \frac{4\pi F^2{}_{\max}}{\int_0^{2\pi}\int_0^{\pi} |F(\theta,\varphi)|^2 \sin\theta d\theta d\varphi} \tag{2-3}$$

We note that an isotropic radiator with F= constant gives D=1.

Power gain is the ratio of the intensity in a given direction to the radiation intensity that would be obtained if the antenna power was radiated isotropically.

We define the parameter e, radiation efficiency, $e = \frac{P_{rad}}{P_{in}}$ (0<e<1). ($P_{in} - P_{rad}$)

represents resistive power losses in the antenna structure. Then, we get the relationship between D and G: G=eD. At microwave frequencies, $e \approx 1$; that means $G \approx D$.

If we know the HPBW in the E plane and H plane, we can use an approximate formula[5] in practice

$$D = \frac{41253}{\theta_E \theta_H}. \tag{2-4}$$

where θ_E and θ_H are measured in degrees.

2.1.3 Polarization

Polarization is defined by the direction of the electric field vector of the wave radiated by the antenna. In practice, polarization of the radiated energy can vary with the direction from the center of the antenna. It is classified as linear, circular or elliptical polarization. For the linear case, $\vec{E}$ lies in a plane; in the circular case, the tip of the $\vec{E}$ vector traces out a circle, and elliptical polarization corresponds to tracing out an ellipse.

2.1.4 Input Impedance

Input impedance is defined as the impedance presented by an antenna at its terminals. It is the ratio of the voltage to current at the pair of terminals, or the ratio of the appropriate components of the electric to magnetic fields at a point. Obviously, this

parameter affects the impedance match between the antenna and receiver, RF amplifier, or transmitter power amplifier. It affects the power transmitted and efficiency of the system.

2.2 Antenna Measurements

In antenna measurements, we should satisfy the minimum distance requirement to measure far field parameters and minimize the reflection effects of ground.

Usually, the minimum distance R which satisfies far field is $R \geq \frac{2D^2}{\lambda}$. Here, D is the aperture diameter, and λ is the wavelength.

On a flat surface as shown in Figure 2.1, an elevation range is chosen to decrease the effect of ground reflection. r is the distance between the two antennas, and h is the elevated height. If the antenna radiated power is confined to a beamwidth of a degrees, the minimum height of the antenna should be $h = \frac{r}{2}\tan\frac{a}{2}$.

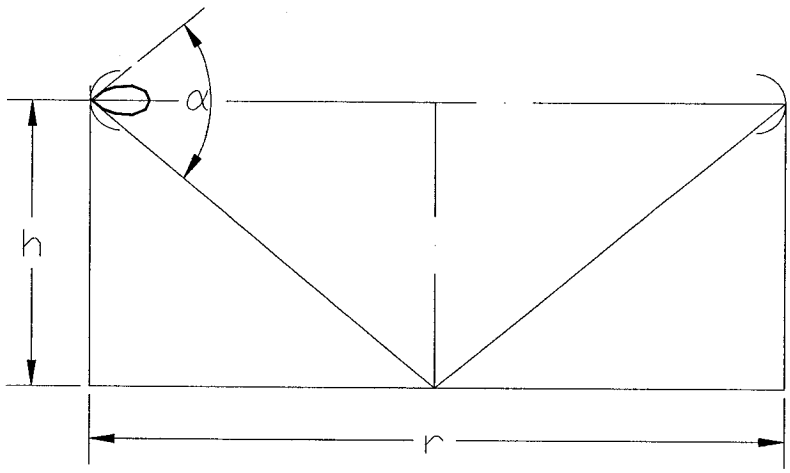

Figure 2.1 Elevated range geometry.

2.2.1 Gain Measurement

Two kinds of methods are used to measure gain: The first method requires two identical antennas. The second method, the gain-comparison method, requires having a standard reference antenna, with a known gain.

Figure 2.2 shows the measurement system for the gain of an antenna[7].

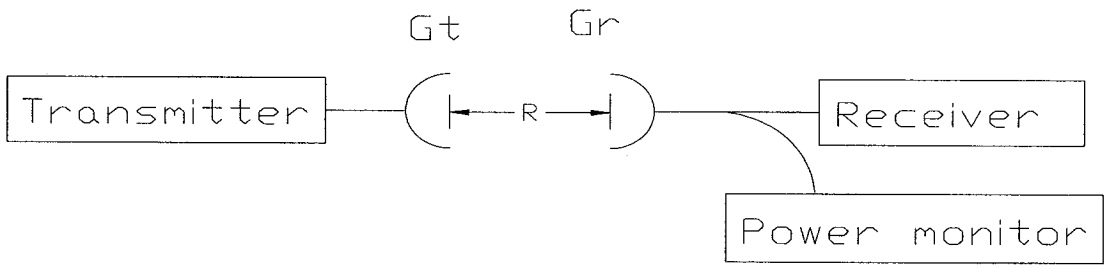

Figure 2.2 Measuring gain of the antenna.

In either case, we have the Friis formula:

$$P_r = \frac{P_t G_t G_r \lambda^2}{(4\pi R)^2} \quad . \tag{2-5}$$

R is the distance between the two antennas. The formula is valid when both antennas are matched, the polarizations are aligned, and far field conditions are respected for both antennas. It is assumed that only one direct ray carries power from the transmitter to the receiver, and that no other paths from reflection or diffraction are present. So if we have two identical antennas with the same characteristics, we can assume that $G_t = G_r$ .Then

$$G_t = G_r = \frac{20\log(4\pi R/\lambda) + 10\log(P_r/P_t)}{2}(dB). \tag{2-6}$$

On the other hand, if we have a standard gain antenna, we can use the gain-comparison method. Using a fixed transmitter power P_t for the source antenna, then firstly, we measure the received power P_s at the standard gain receive antenna with

a known gain G_s; secondly, we measure the power P_u received by the unknown gain antenna. Comparing the difference between P_s and P_u, we can measure the unknown gain G_u

$$G_u = \frac{P_u}{P_s} G_s \quad . \tag{2-7}$$

2.2.2 Impedance Measurement

We can measure the S parameter of the system by using a network analyzer conveniently. When all the ports are matched, $S_{11} = \Gamma$. Γ is the reflection coefficient. The phase of S_{11} can also be measured, so that we can obtain the complex value of the antenna input impedance Z_{ant}. Z_{ant} and Γ are related by

$$\begin{aligned} \Gamma &= \frac{Z_{ant} - Z_0}{Z_{ant} + Z_0} \\ Z_{ant} &= Z_0 \frac{1+\Gamma}{1-\Gamma} \end{aligned} \tag{2-8}$$

Usually, we use the term return loss (RL) to describe the power loss caused by the impedance mismatch. It is defined as

$$RL = -20 \log |\Gamma| \, dB \quad . \tag{2-9}$$

so when the measured S parameter recorded in decibel, $RL = -|S_{11}|$.

2.3 Helix antenna

A helix antenna is a high gain circular polarization antenna. It was invented by John Kraus in 1946 and he found that the directivity and center frequency of the helix antenna can be adjusted by the antenna geometry[8]. Now, the helix antenna has become one of the most popular circularly polarized antennas used in industry.

2.3.1 Helix antenna theory

The geometrical description of the helix is in terms of N turns, diameter D, and spacing of each turn S. This is shown in Figure 2.3.

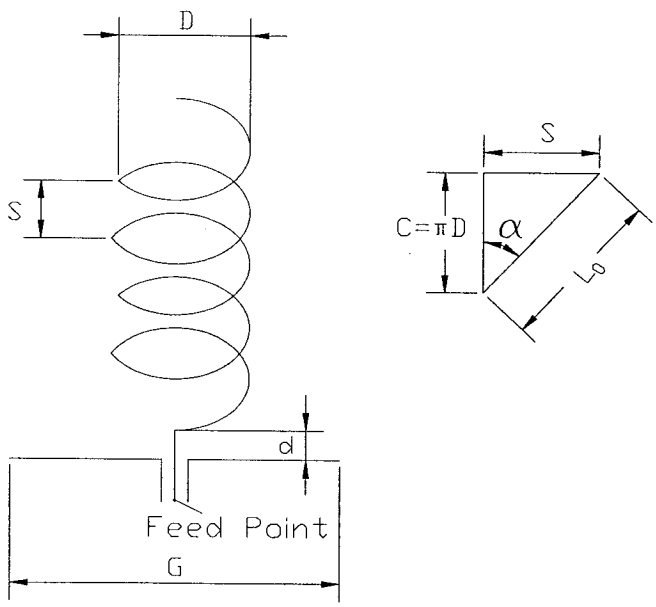

Figure 2.3 Helix antenna.

It operates on a ground plane that can be circular or square. The feed point is connected to a coaxial cable. The center conductor of the cable is connected to the helix and the shield is connected to the ground plane. The parameters for the design are:

Circumference $C = \pi D$

Length of conductor in one turn $L_0 = \sqrt{C^2 + S^2}$

Pitch angle $\alpha = \tan^{-1}(\frac{S}{C})$.

Usually, we select N>3, 3/4<C/λ<4/3, $12^\circ < \alpha < 14^\circ$.

In practice, we may have[9]

Circumference $C_\lambda = 0.75 \sim 1.33\lambda$

Spacing of each turn $S_\lambda = 0.2126 \sim 0.2867 C_\lambda$

Ground plane diameter $SL = 0.8 \sim 1.1\lambda$

Input impedance $R = 140 C_\lambda$ (2-10)

Directivity $D \cong 15N\frac{C^2 S}{\lambda^3}$ (2-11)

Gain in dBi $G = 11.8 + 10\log(C_\lambda^2 N S_\lambda)$ (2-12)

Half power beamwidth $HPBW = \frac{52^\circ}{C_\lambda \sqrt{N S_\lambda}}$ (2-13)

First null beamwidth $FNBW = \frac{115^\circ}{C_\lambda \sqrt{N S_\lambda}}$. (2-14)

For a Hansen-Woodyard end-fire radiation mode, the normalized far-field pattern is

$$E = \sin(\frac{\pi}{2N})\cos\theta\frac{\sin[(N/2)\psi]}{\sin(\psi/2)} \quad . \qquad (2\text{-}15)$$

In (2-15),

$$\psi = k_0(S\cos\theta - \frac{L_0}{p})$$
$$p = \frac{L_0/\lambda_0}{S/\lambda_0 + [(2N+1)/2N]}. \qquad (2\text{-}16)$$

2.3.2 Numerical Technique

Many mathematical methods have been developed to solve the electromagnetic problem. In this section, we will talk about one of the numerical techniques — moment method.

2.3.2.1 Moment Method

The moment method (MM) for electromagnetic problems began rapid development in the 1960's. The technique was described by R.F. Harrington "Field Computation by Moment Methods" in 1968[10]. We will use the MM to predict the radiation pattern and impedance of helical antenna designs. To understand the concept behind the MM, we will discuss its application to a straight wire, as shown in Figure 2.4. A more general development, permitting an arbitrary network of short straight wire segments, has been implemented in a general purpose computer code, known as the Numerical Electromagnetics Code (NEC)[11]. This code is further discussed in Section 2.3.2.2.

Returning to the straight wire in Figure 2.4, one finds that the wire current is

required to satisfy an integral equation of the form

$$\int I(z')K(z,z')dz' = -E_z^{\,i}(z). \tag{2-17}$$

By applying the MM to (2-17) we can obtain a system of simultaneous linear algebraic equations in terms of the unknown current $I(z')$. $K(z,z')$ is known as the kernel, and is related to a Green's function for the electric field. By solving the linear equations, the current is obtained. Once the current is known, it is easy to determine the radiation pattern and impedance. When analyzing wire antenna such as the dipole and helix, this method can offer excellent results.

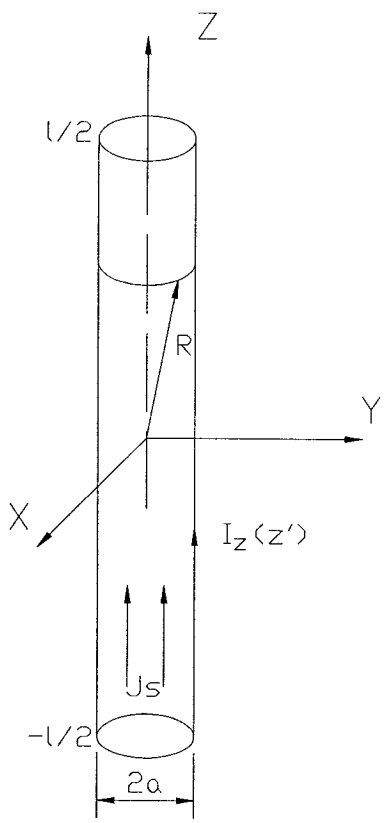

Figure 2.4 Straight wire with current $I(z')$.

Assume the straight wire is of radius a, and located on the z axis from $-l/2$ to $l/2$. In free space, the boundary condition on the tangential electric field is $E_z^{\,t}(r) = E_z^{\,i}(r) + E_z^{\,s}(r)$. At the surface of the perfectly conducting wire and also the interior to the wire, the sum of E_z^s and E_z^i must be zero, i.e.

$$E_z^s = -E_z^i. \tag{2-18}$$

From the Lorentz gauge condition, we have

$$\Phi = -\frac{1}{j\omega\mu\varepsilon}\frac{\partial A_z}{\partial z} \tag{2-19}$$

where Φ is the scalar potential and A_z is the magnetic vector potential. From potential theory, the $\vec{E}$ produced by the current J_z is $\vec{E} = -j\omega\vec{A} - \nabla\Phi$.

So

$$E_z^s = -j\omega A_z - \frac{\partial\Phi}{\partial z}. \tag{2-20}$$

Substituting equation (2-19) into (2-20), we obtain

$$E_z^s = \frac{1}{j\omega\mu\varepsilon}\left(\frac{\partial^2 A_z}{\partial z^2} + \beta^2 A_z\right). \tag{2-21}$$

Because it is a thin wire, we can neglect the radial current density J_ϕ and just consider axial current density J_z. Hence, the vector potential A_z is given by

$$A_z = \frac{\mu}{4\pi}\int_{-l/2}^{l/2}\left[\int_0^{2\pi} J_z \frac{e^{-j\beta R}}{R} a\,d\phi'\right]dz'. \tag{2-22}$$

Since

$$I(z') = 2\pi a J_z \tag{2-23}$$

(2-22) becomes

$$A_z = \mu \int_{-l/2}^{l/2} I(z')[\frac{1}{2\pi} \int_0^{2\pi} \frac{e^{-j\beta R}}{R} d\phi']dz' . \tag{2-24}$$

If we define

$$G(z,z') = \frac{1}{2\pi} \int_0^{2\pi} \frac{e^{-j\beta R}}{R} d\phi' \tag{2-25}$$

then (2-24) becomes

$$A_z = \mu \int_{-l/2}^{l/2} I(z')G(z,z')dz' . \tag{2-26}$$

If one observes the E-field due to the surface current distribution at a point on the wire axis, we have that $R \approx \sqrt{(z-z')^2 + a^2}$. From (2-18), (2-21) and (2-25), we get the integral equation for the unknown $I(z')$ as

$$\frac{1}{j\omega\varepsilon_0} \int_{-l/2}^{l/2} I(z')[(\frac{\partial^2}{\partial z^2} + \beta^2)G(z,z')]dz' = -E_z^i \quad . \tag{2-27}$$

We may write (2-27) in the form

$$F(g) = h . \tag{2-28}$$

F is an integrodifferential operator, h is a known excitation function, and g is the response function. Once F and h are specified, g can be determined. We assume that the unknown g can be expanded as

$$g(z') = \sum_{n=1}^{N} a_n g_n(z') \quad . \tag{2-29}$$

The g_n are a suitable set of basis functions; a linear combination can represent g . Each a_n is a complex expansion coefficient and each $g_n(z')$ is a known function usually referred to as a basis or expansion function. Substituting (2-29) into (2-28), we get

$$\sum_{n=1}^{N} a_n F(g_n) = h_m \qquad m = 1,2,...,N. \tag{2-30}$$

$h_m = h(z_m)$ represents sample values of h at points z_m. Hence, (2-28) is being enforced at the points $z = z_1, z_2, ..., z_M$. This technique is called "point matching" or "collocation." In matrix from, the equation can be written as

$$[V_m] = [Z_{mn}][I_m] \tag{2-31}$$

where

$$Z_{mn} = F(g_n)$$

$$I_n = a_n$$

$$V_m = h_m.$$

Thus we get the unknown current distribution by solving the matrix equation

$$[I_n] = [Z_{mn}]^{-1}[V_m] \quad . \tag{2-32}$$

2.3.2.2 NEC Code

The Numerical Electromagnetics Code (NEC) is an implementation of the MM[11]. It is able to solve for the currents on arbitrarily shaped wires, and wire junctions, in any general combination. Besides allowing us to model dipoles and helix antennas, we can model solid metal surfaces by constructing a wire grid model. The ability to model wires and metal surfaces allows us to find out how metal structures radiate and scatter electromagnetic fields.

Frequently we use a wire grid to simulate an actual continuous metal body. When the grid size becomes small relative to the wavelength, the grid supports a current distribution which approximates that on the corresponding continuous surface. The rule of thumb is that the surface of the wires parallel to one linear polarization is made equal to the surface of the solid surface being modeled. It is called "same surface area rule," that is, for a square wire grid, suitable for any polarization, the total surface area of the wires is then twice the area of the solid surface.

NEC is able to analyze an arbitrary structure of wires in free space or over a ground plane by using the moment method. It models the metal structure as small straight segments and then obtains the currents on the segments. When we make a wire grid, it should obey some basic rules. Generally, the segment length Δ should be in the range of $0.05 < \Delta < 0.2\lambda$, too long or too small a length will cause more error[11]. When Δ/radius of wire is greater than 8 or less than 1%, it will cause errors. Table 2.1 is the summary of "modeling guidelines" which is an excerpt from the paper "Verifying wire-grid model integrity with program 'check' " [12].

Table 2.1 Summary of modeling guidelines.

		Warning	Error
Individual segments	Segment length	$0.1 < \Delta < 0.2\lambda$	$\Delta > 0.2\lambda$
	Radius	$30 < \lambda / a < 100$	$\lambda / a < 30$
	Segment to radius ratio	$0.5 < \Delta / a < 2$	$\Delta / a < 0.5$
Junctions	Segment length ratio		$\Delta_{big} / \Delta_{small} > 5$
	Radius ratio	$5 < a_{big} / a_{small} < 10$	$a_{big} / a_{small} > 10$
	Segment to radius ratio	$2 < \Delta / a < 6$	$\Delta / a < 2$
	Match point	Segment center within half a wire radius of another wire's surface	Segment center lies within the volume of another wire

Δ=segment length; a=wire radius; λ=wavelength.

2.3.2.3 Comparison of a NEC Model and Approximate Models for a Helix

NEC2 solves an integral equation for the wire currents, and the solution is quite exact. In this work, NEC2 was used to model a helical antenna and its ground plane. To establish confidence in our modeling technique, we first examined an antenna for which a measured pattern has been published. We examined an 8 GHz helix antenna, with

$N=10$, $\alpha=13^{\circ}$, $l_0=0.92\lambda=3.45cm$, $s=0.796cm$. We have the measured E_ϕ field pattern from [13] and it is shown in Figure 2.5. The measured HPBW is 45° and the gain is about 12 dB.

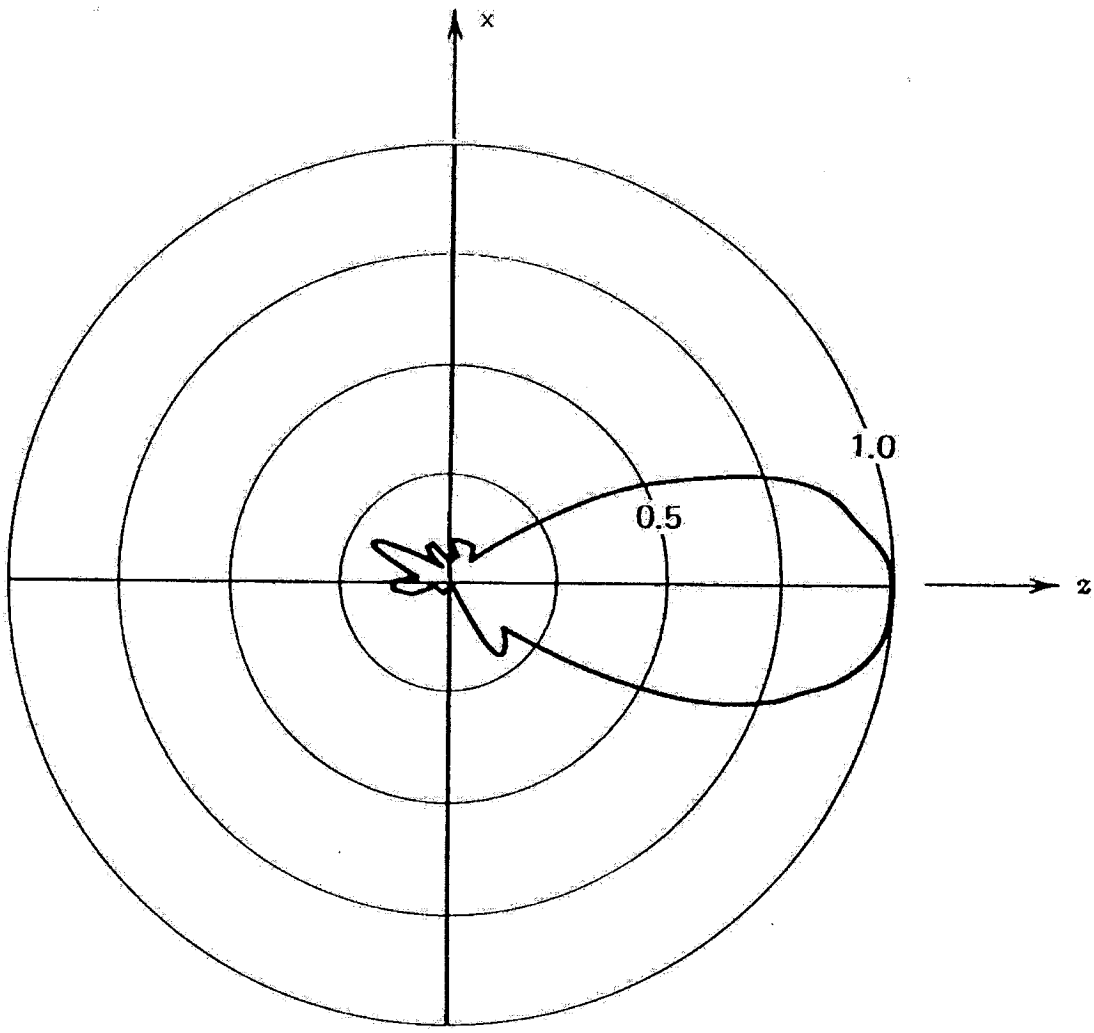

Figure 2.5 Measured E_ϕ of 8 GHz antenna[13], E_θ on a linear scale.

The NEC result for the radiation pattern was in good agreement with the measured result and the calculation result which gets from the approximate formula from W. L. Stutzman and G. A. Thiele[14]. A square wire grid model with 0.1λ segments was constructed for the ground plane, and short straight segments were used for the helix. The wavelength at 8 GHz is 3.75 cm, and the ground plane size was one λ by one λ, i.e. 3.75 cm by 3.75 cm square. Because the segment length was 0.1λ, each wire was divided into 10 segments, that is the mesh was made from 11 by 11 wires. Then following the "same surface area" rule, the relationship between the wire radius and the dimension of the ground is

$$11 \times 2\pi a = \lambda = 10\Delta = 3.75$$

thus the wire radius $a = 0.54\,mm$.

Figure 2.6 shows the wire grid model, and the NEC input file for the 8 GHz antenna is shown in Table 2.2. We obtained $G = 12.4dB$, and $HPBW = 42^\circ$.

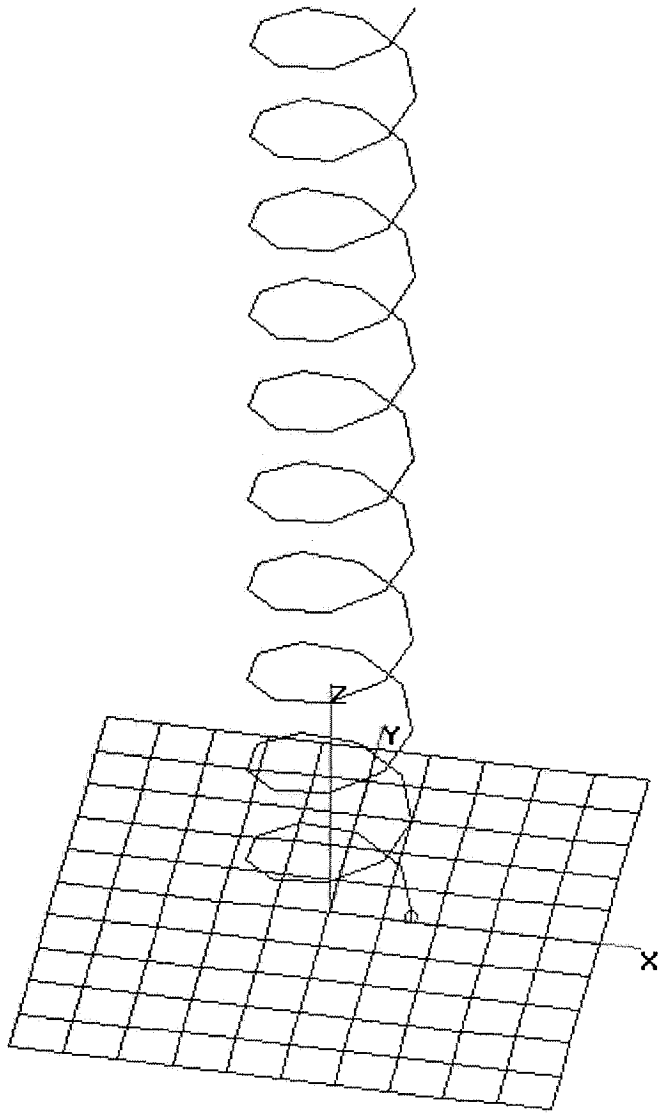

Figure 2.6 Wire grid model of 8 GHz helix antenna.

Table 2.2 NEC input file for 8 GHz helix antenna on finite ground plane.

```
CM  5    10    15    20          30          40          50          60          70          80
CM 8000MHz HELIX WITH N=10 LO=3.45CM S=0.796CM
CM FC is 8000MHz WL=3.75cm wire radius is 0.5mm
CM USE 1 WAVELENGTH PLANE GRID BY 0.1WL SO WR=WL/22PI=0.054CM
CE
SY  F=8000
SY  LH=0.0796
SY  L=0.0345
SY  D=0.00535
SY  R=.0005
SY  WR=0.00054
SY  S=0.00796
SY  H=0.001
GH 88   90          S          LH          D           D           D           D           R
GM 88    0          0           0          0           0           0           H
GW  1   10       -L/2        -L/2          0         L/2        -L/2           0          WR
GW  2   10       -L/2        -2L/5         0         L/2        -2L/5          0          WR
GW  3   10       -L/2       -3L/10         0         L/2       -3L/10          0          WR
GW  4   10       -L/2        -L/5          0         L/2        -L/5           0          WR
GW  5   10       -L/2       -L/10          0         L/2       -L/10           0          WR
GW 60    6       -L/2           0          0        L/10           0           0          WR
GW 61    1       L/10           0          0           D           0           0          WR
GW 62    1          D           0          0         L/5           0           0          WR
GW 63    3        L/5           0          0         L/2           0           0          WR
GW  7   10       -L/2        L/10          0         L/2        L/10           0          WR
GW  8   10       -L/2         L/5          0         L/2         L/5           0          WR
GW  9   10       -L/2       3L/10          0         L/2       3L/10           0          WR
GW 10   10       -L/2        2L/5          0         L/2        2L/5           0          WR
GW 11   10       -L/2         L/2          0         L/2         L/2           0          WR
GW 12   10       -L/2        -L/2          0        -L/2         L/2           0          WR
GW 13   10      -2L/5        -L/2          0       -2L/5         L/2           0          WR
GW 14   10      -3L/10       -L/2          0       -3L/10        L/2           0          WR
GW 15   10       -L/5        -L/2          0        -L/5         L/2           0          WR
GW 16   10      -L/10        -L/2          0       -L/10         L/2           0          WR
GW 17   10          0        -L/2          0           0         L/2           0          WR
GW 18   10       L/10        -L/2          0        L/10         L/2           0          WR
GW 19   10        L/5        -L/2          0         L/5         L/2           0          WR
GW 20   10      3L/10        -L/2          0       3L/10         L/2           0          WR
GW 21   10       2L/5        -L/2          0        2L/5         L/2           0          WR
GW 22   10        L/2        -L/2          0         L/2         L/2           0          WR
GW 30    1          D           0          H           D           0           0          R
GE  0
EX  0   30    1    0          1.          0.          0.          0.          0.          0.
FR  0    1    0    0        8000          50
RP  0  361    1 1001           0           0           1           0
EN
```

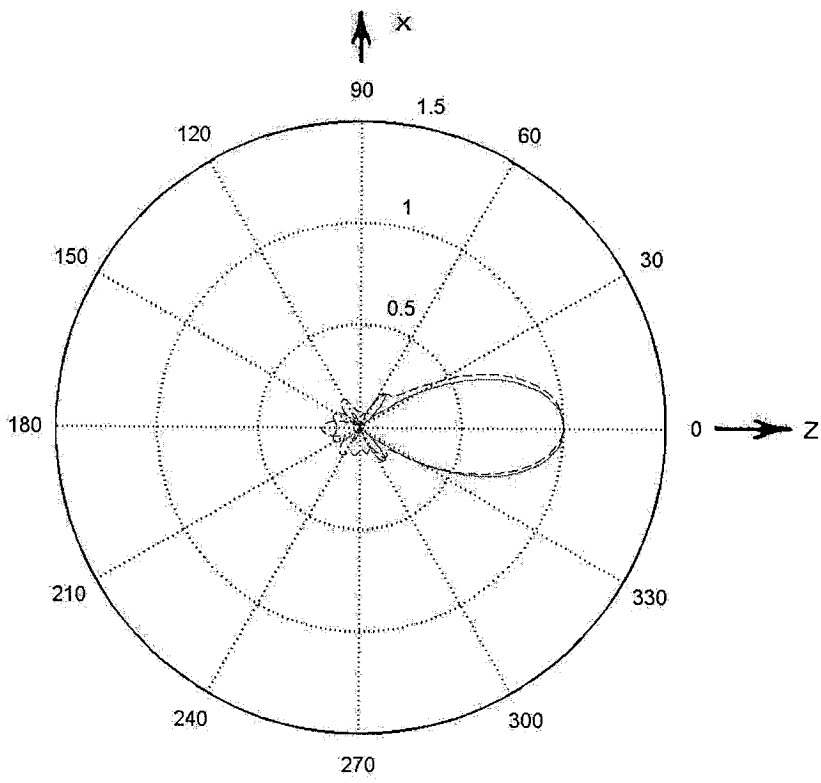

Figure 2.7 E_θ from NEC2 model and (2-15), E_θ on a linear scale.

--- NEC2 result, — (2-15) result

The calculated E_θ field pattern was also computed from (2-15). We get $HPBW = 39^\circ$ and $D = 14dB$. The normalized radiation patterns from NEC2 and (2-15) are shown in Figure 2.7 together. The pattern agrees well with the NEC2 model and the theoretical result.

Table 2.3 is the comparison of these results for the measured results, the NEC2 simulation with a square grid ground plane, and the simple formula (2-15).

Table 2.3 Comparison of results for 8 GHz helix.

	HPBW(°)	Error	Gain(dB)
Measured result	45	---	12
NEC2 model	42	6.7%	12.4
(2-15) Result	39	13.3%	14.3

From Table 2.3, we can find that the angle of HPBW from the NEC2 model has less error than the approximate theoretical calculation result from (2-15). We also find the gain obtained from the NEC2 model and theoretical calculation are in close agreement.

2.3.3 Input Impedance Matching

Typically, the input impedance of a helix is about 150 Ohms, but for the system, the feed impedance is usually 50 Ohms, so we need to match this impedance. The 50-ohm matching method was introduced by Kraus in 1977[15]. It lowers the characteristic impedance of the conductor-ground plane combination by using a wide metal foil soldered to the helix, between the feed point and the beginning of the helix conductor. Figure 2.8 shows the structure of the match.

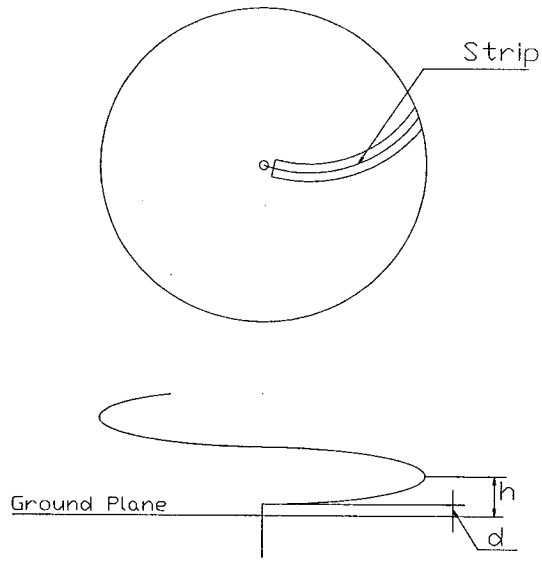

Figure 2.8 Structure of the matching section.

The strip acts as a transmission line, so it works as a continuous taper transformer. It seems reasonable to model the transformer by using the theory of small reflections[16], so we decided to try that approach. Figure 2.9 is the example of a tapered transmission line matching section. As shown in Figure 2.9 (b), a section of line ΔZ would have a reflection coefficient

$$\Delta\Gamma = \frac{(Z+\Delta Z)-Z}{(Z+\Delta Z)+Z} \approx \frac{\Delta Z}{2Z}. \tag{2-33}$$

In the limit as $\Delta Z \to 0$, we get the differential:

$$d\Gamma = \frac{dZ}{2Z} = \frac{1}{2}\frac{d(\ln Z / Z_0)}{dz}dz. \tag{2-34}$$

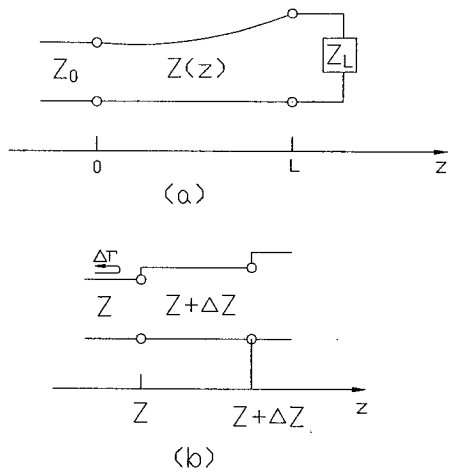

Figure 2.9 A tapered transmission line matching section (a) Continuous tapered transmission line section. (b) Model for an incremental step changes in impedance of the tapered line.

Since

$$\frac{d(\ln f(z))}{dz} = \frac{1}{f}\frac{df(z)}{dz}$$

the total reflection coefficient at the input can be obtained:

$$\Gamma(\theta) = \frac{1}{2}\int_{z=0}^{l} e^{-2j\beta z}\frac{d}{dz}\ln(\frac{Z}{Z_0})dz \qquad (2\text{-}35)$$

where $\theta = 2\beta l$. With different f, we can plot Γ vs. frequency. The characteristic impedance $Z(z)$ at the terminals at $z = 0$, can then be found from (2-9).

2.4 Parabolic Reflector Antenna

At microwave frequencies, people use reflector antennas mostly because they have high directivity. A reflector antenna consists of two parts: feed and reflector. The feed is the electromagnetic wave point source and the reflector provides the gain. Reference [17] surveys more details for all kinds of reflectors, and discusses the numerical calculation methods, for reflector antennas.

2.4.1 Geometry of Prime-focus Parabolic Antenna

A prime-focus parabola is formed by rotating the arc of a parabola about the line joining the vertex and the focal point. Usually, the geometrical characteristics consist of the focal length f, and surface diameter D. We have

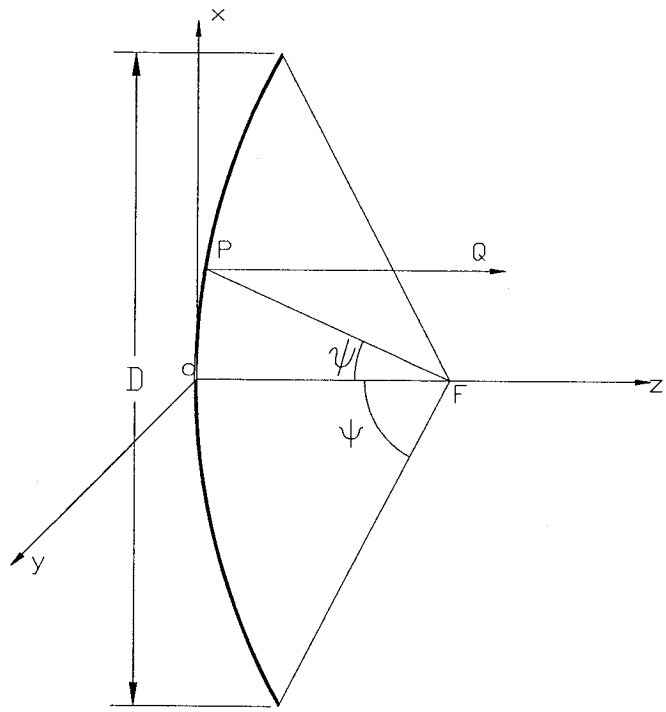

Figure 2.10 Geometric structure of parabolic reflector.

$$x^2 + y^2 = 4fz \tag{2-36}$$

$$p = \frac{2f}{1+\cos\theta} = f\sec^2\frac{\theta}{2} \ . \tag{2-37}$$

The relationship between f and D is

$$\frac{f}{D} = 0.25\cot\frac{\theta_0}{2} \ . \tag{2-38}$$

There are two important characteristics of parabolic surface:

(A) All the reflected rays transmitted from the focus are parallel.

(B) The sum of the distance from any point on the parabolic curve to the focus, and the distance from the point to the directrix always equals two times the focal distance.

2.4.2 Feed of Parabolic Antenna

The feed of the reflector antenna should provide a suitable illumination pattern for the reflector. It should satisfy these conditions:

(A) It has one symmetric main lobe with 10dB beamwidth equal to the angle of the parabola rim.

(B) It has a well defined phase center.

(C) It is matched to the receiver.

(D) It offers little blockage to the reflector.

2.4.3 Gain of Reflector Antenna

A parabolic reflector antenna has high directivity. It is possible to get an accurate solution for the field distribution of a reflector antenna, but we will find it adequate to use some simple formulas to estimate the gain of the reflector,

$$\text{Gain } G_e = \varepsilon_{ap}(\frac{\pi D}{\lambda})^2 . \tag{2-39}$$

D is the diameter of the aperture, and ε_{ap} is the aperture efficiency. Generally, ε_{ap} is about 50%~60%, and the typical efficiency is 55%[18], So in (2-39) we let $\varepsilon_{ap} = 0.55$.

2.4.4 Offset Reflector

In practice, a satellite ground station often uses an offset parabolic reflector as in Figure 2.11 by intercepting a part of a normal parabola curve. The advantage of this structure is that the blockage effect of the feed is minimized and this will improve the performance of the antenna.

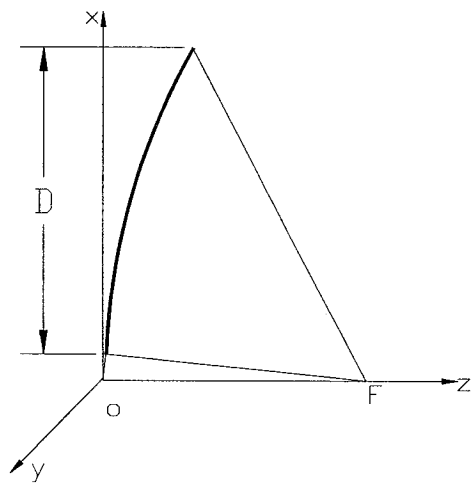

Figure 2.11 Structure of offset antenna.

Chapter 3

Downlink Antenna Design and Testing

3.1 Downlink Reflector Antenna Feed

A horn, dipole, helix, etc… can be used as the feed for a parabolic reflector antenna. Each kind of feed has its advantages and disadvantages. A helix was selected because it is easy to fabricate. It is inexpensive, has low aperture blockage, a constant beamwidth over a broad band in the two principal planes, good pattern symmetry, and low side lobes. It is compatible with the circular polarization used by the AO-40 satellite.

3.1.1 Feed Design

At 2.4 GHz, the wavelength is 12.5cm. The illumination angle of the parabola antenna is about 77^0 (See Appendix A). From (2-10) to (2-14), the geometric dimensions for the helix are given in Table 3.1.

Table 3.1 Geometric dimension of 2.4 GHz helix feed antenna[19].

Parameter		Ratio vs. wavelength
Turns N	5.75	---
Wavelength λ	12.5 cm	---
Diameter of each turn D	4.6 cm	---
Spacing of each turn S	3 cm	0.24λ
Circumference C	14.44 cm	1.155λ
Ground plane side length SL	12.5 cm	λ
Pitch angle α	12^0	---

After deciding on the geometrical dimensions of the helix, we can build it, and simulate the performance. The ground plane is square.

3.1.2 Helix Assembly

To make the feed, we used these materials: one thin 12.5 by 12.5 cm aluminum plate, and 3mm diameter copper wire for the helix, copper foil to make a 1/4 arc matching section. We obtained much helpful information from [20] to make the helix feed. To make the helix, these steps were followed:

(A) Drill the ground plane as in Figure 3.1.

(B) Trim the copper foil as in Figure 3.1. Prepare some different sizes of the width

and length of the foil, replace these in the measurement and select the best one.

(C) The helix is wound left hand circular polarized (LHCP) because it is reflected in the dish and will become RHCP.

(D) Solder the matching arc.

(E) Install the N connector on the ground plane.

(F) Solder the helix, being careful with the distance between the last turn of the helix and the ground plane.

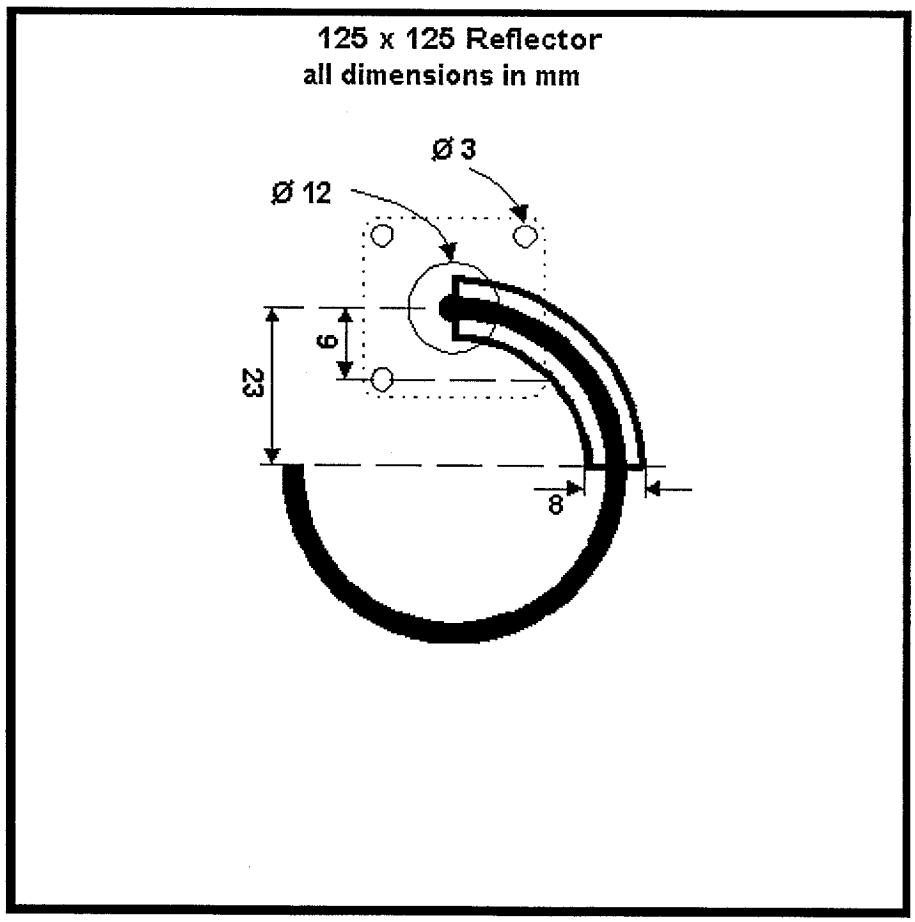

Figure 3.1 Dimensions for ground plane and matching section[20].

Figure 3.2 is the picture of the helix feed.

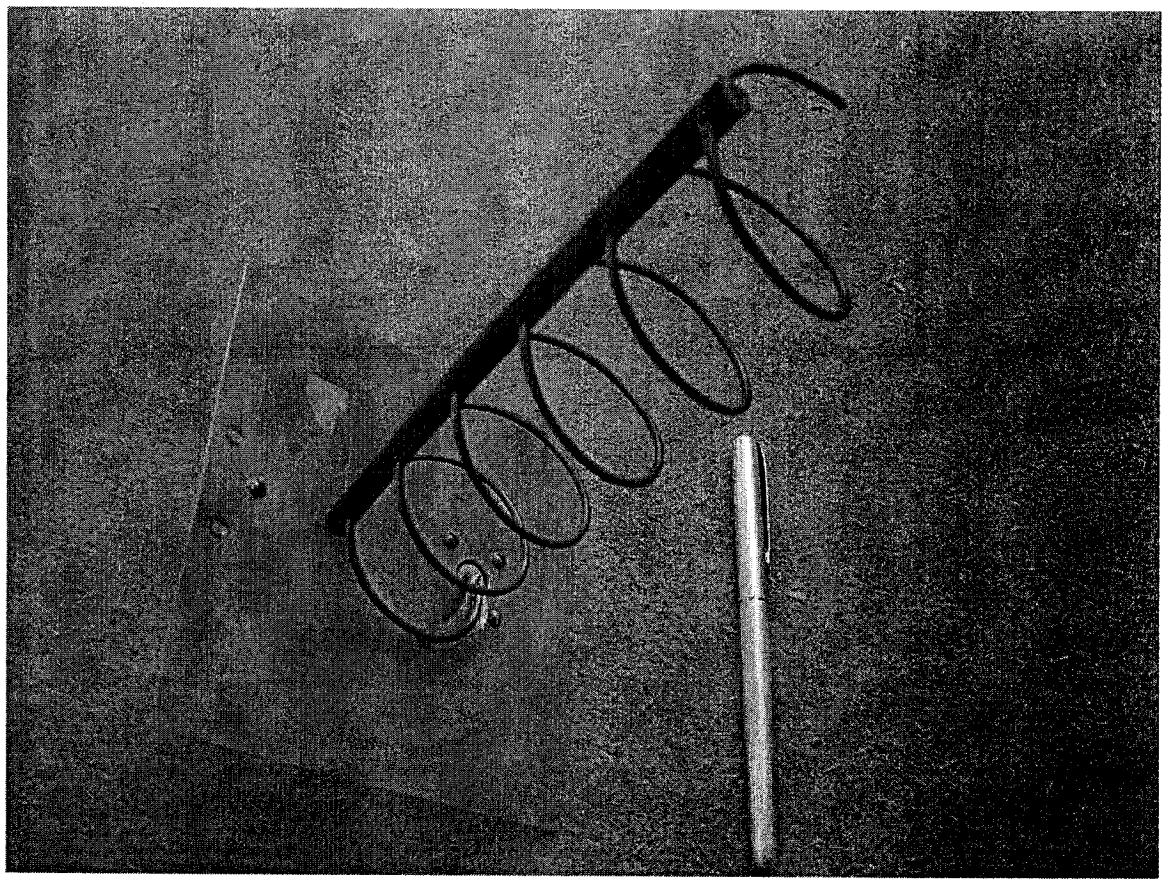

Figure 3.2 Assembled 2.4 GHz helix feed.

3.1.3 Feed Measurement Results

This section gives the reflector coefficient and gain measurement results of the 2.4 GHz helix antenna.

3.1.3.1 Return loss measurement

Figure 3.3 is the measurement system to measure the antenna impedance. We used a Hewlett Packard 8410C network analyzer.

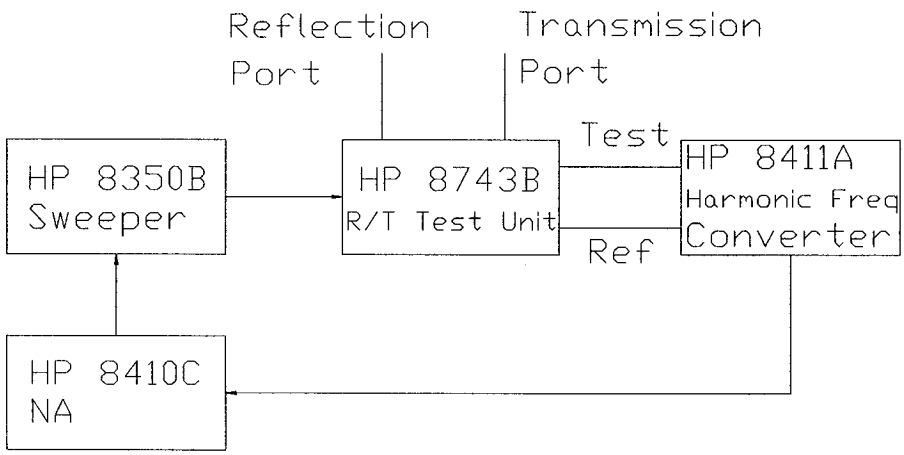

Figure 3.3 2.4 GHz helix RL measurement system.

We repeat the RL measurement by trying different size matching sections, and selecting the one which has the best RL. At last the selected matching section has the width of 0.8cm and length of a quarter turn. Figure 3.4 shows the measurement result. In Figure 3.4, we see that from 2.3 GHz to 2.47 GHz, RL>10 dB. At downlink operation frequency, i.e. 2401 MHz, RL>18 dB.

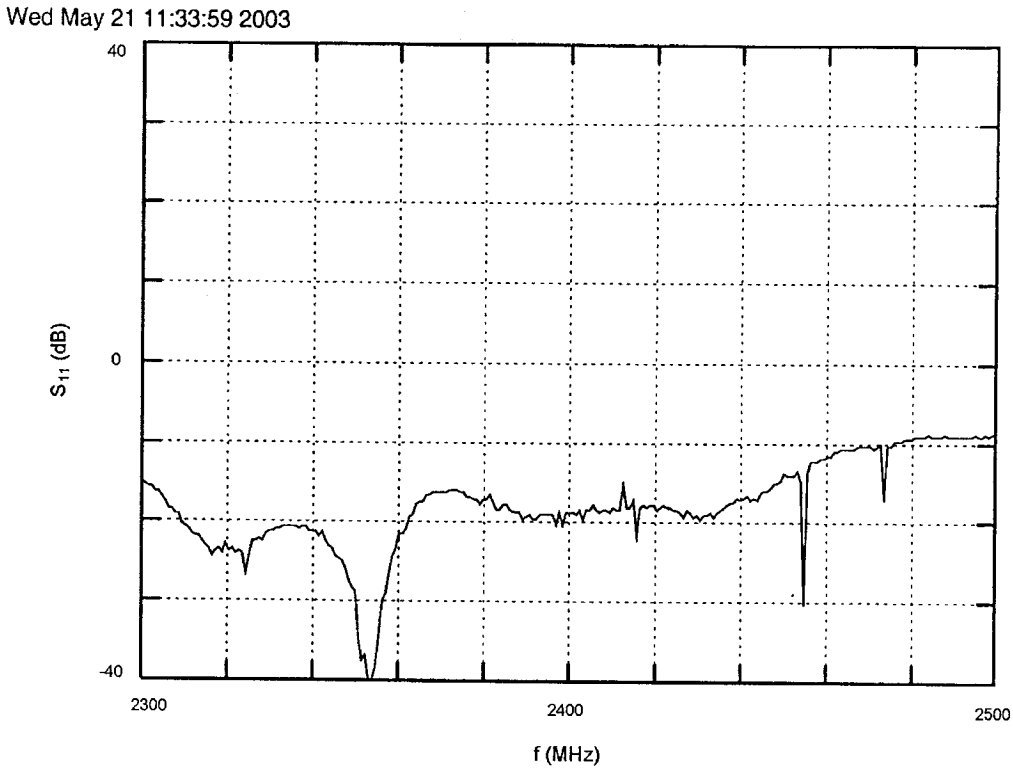

Figure 3.4 S_{11} measured result for 2.4 GHz helix, 10 dB/div.

3.1.3.2 Gain Measurement

The gain-comparison method was used to measure the gain of the helical feed antenna. Figure 3.5 shows the gain measurement system.

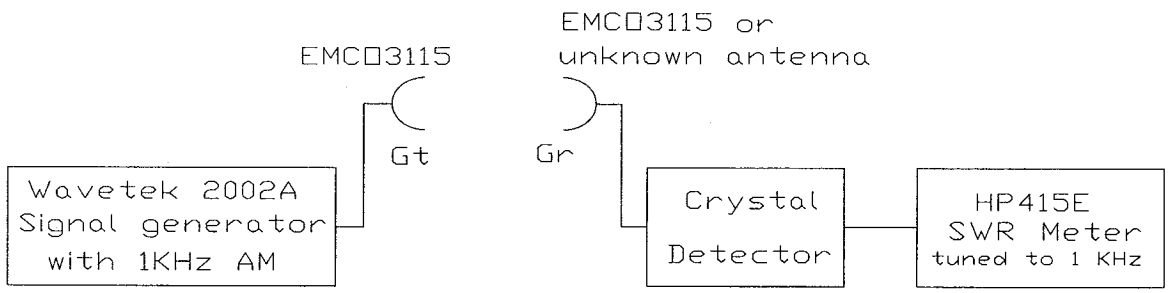

Figure 3.5 Gain measurement using gain-comparison method.

In the experiment, an EMCO 3115 antenna, which is a wideband (1-18 GHz) ridged waveguide antenna, was selected as the standard antenna. Because of limited lab space, it was not possible to set up our microwave absorber panels. The measurement was just done in free space, on the lab bench. The maximum dimension of the helix is about 18cm, so the minimum measurement distance is about $R \geq \frac{2D^2}{\lambda} \approx 52cm$. We used a distance between the two antennas as 2m, and a height of 1m. By comparing with the gain of the EMCO 3115 antenna, the gain of the helix antenna was obtained. Table 3.2 gives the measurement results. In absolute terms, the dB readings have no specific significance. It is the difference that gives us the gain.

Table 3.2 Measurement data of G_r for helix feed, at 2.4 GHz.

	Data from SWR meter
G_r by using EMCO 3115	43.6 dB
G_r by using unknown helix	44.1 dB

The performance of the EMCO 3115 double ridged guide antenna is shown in Appendix B. It has a gain of 9dB at 2.4 GHz. After replacing the EMCO 3115 antenna by the helix, the gain decreases 0.5 dB; this means that the gain of the 2.4 GHz helix is 8.5 dB. In experiment, the measured error will be caused by many factors, such as polarization loss, power loss, multipath effect, etc. The VSWR of EMCO3115 is about 1.5:1 at 2.4GHz, i.e., reflection coefficient Γ=0.2, so the power loss is about 4%, this will influence the measured result slightly and could be neglected. It is important to note that there is 3 dB polarization loss, so actual gain of helix is 11.5 dB, because the standard gain antenna is linearly polarized and the helical antenna is circularly polarized.

3.1.4 Computer Model of the Feed

This section talks about the computer model for the reflection coefficient of the 2.4 GHz helix with the matching section, and gives the NEC model for the helix.

3.1.4.1 Reflection coefficient with transformer

We can consider the transformer as a microstrip line on dielectric with ε_r=1. The characteristic impedance of this line is[21]

$$Z_0 = \begin{cases} \dfrac{60}{\sqrt{\varepsilon_e}} \ln\left(\dfrac{8d}{W} + \dfrac{W}{4d}\right) & for \dfrac{W}{d} \le 1 \\ \dfrac{120\pi}{\sqrt{\varepsilon_e}\left[\dfrac{W}{d} + 1.393 + 0.667 \ln\left(\dfrac{W}{d} + 1.444\right)\right]} & for \dfrac{W}{d} \ge 1 \end{cases} \qquad (3\text{-}1)$$

$$\varepsilon_e = \frac{\varepsilon_r + 1}{2} + \frac{\varepsilon_r - 1}{2} \frac{1}{\sqrt{1 + 12d/W}}$$

Here, $\varepsilon_e = \dfrac{\varepsilon_r + 1}{2} + \dfrac{\varepsilon_r - 1}{2} \dfrac{1}{\sqrt{1 + 12d/W}} = 1$

so

$$Z_0 = \begin{cases} 60 \ln\left(\dfrac{8d}{W} + \dfrac{W}{4d}\right) & for \dfrac{W}{d} \le 1 \\ \dfrac{120\pi}{\left[\dfrac{W}{d} + 1.393 + 0.667 \ln\left(\dfrac{W}{d} + 1.444\right)\right]} & for \dfrac{W}{d} \ge 1 \end{cases} \qquad (3\text{-}2)$$

With W=8mm, and d=2mm~8mm, the total length of the 1/4 turn arc is about 36mm. Substituting (3-2) into (2-35), we can get

$$\Gamma(\theta)=\frac{1}{2}\int_{z=0}^{z=0.035} e^{-2j\beta z}\frac{0.17W[W+2.111*(0.17*z+d_0)]}{[W+1.393(0.17*z+d_0)+0.667*\ln(\frac{W}{0.17*z+d_0}+1.444)]*[W+1.444(0.17*z+d_0)]*(0.17*z+d_0)}dz \tag{3-3}$$

by using MATLAB, we can evaluate the integral numerically. We can get the impedance of the helix without matching from (2-10), then we can also get the reflection coefficient from (2-8). Figure 3.6 shows the predicted return loss with the matching network and without it. We see that for this matching network, a return loss of better than 12 dB is predicted. Without the matching network, the 160Ω helical antenna on a 50Ω line would give a return loss of about 6 dB.

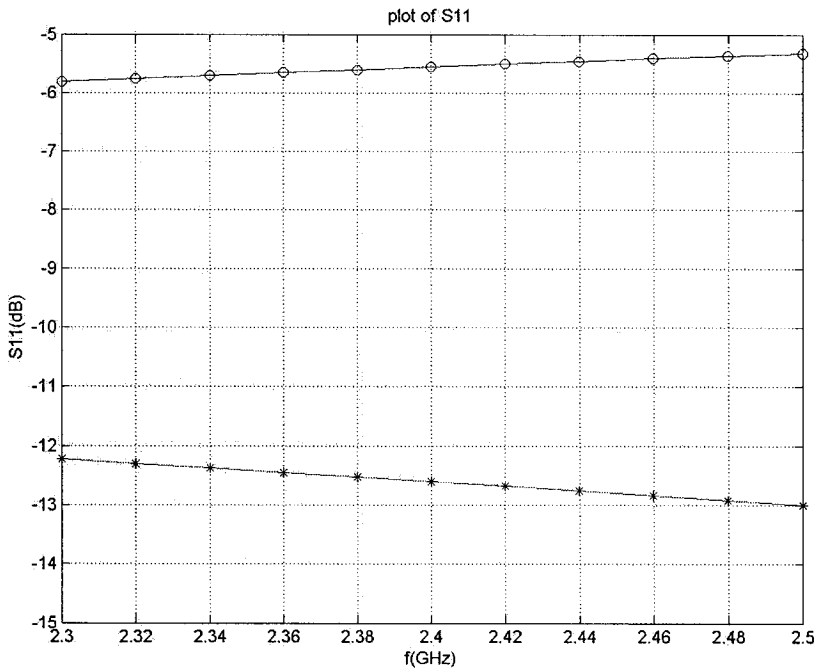

Figure 3.6 Theoretical S_{11} of 2.4 GHz helix.

* S_{11} with matching network, ∘ S_{11} without matching.

3.1.4.2 NEC Simulation Result

We modeled the 2.4 GHz helix, without the matching section. A preliminary investigation revealed that modeling the matching network is difficult, probably because the large feed currents require a very accurate model of the geometry. For this reason, it was omitted.

Figure 3.7 and Figure 3.8 give the radiation pattern and current distribution respectively, for the 2.4 GHz helix feed. Table 3.3 shows the comparison of the NEC2 model, experimental results and theoretical calculation using (2-11)—(2-14). We also provide the NEC2 input file and brief output file in Appendix C and Appendix E respectively.

Table 3.3 Comparison of results for 2.4 GHz helix.

	HPBW(^{0})	Gain(dB)	Impedance(Ω)
Measured result	---	11.5	---
NEC2 model	43	11.4	137-j62
(2-11)-(2-14) calculation	38	14.4	162+j0

From Table 3.3, we find that the results are rather good. The computer model and

experiment obtain similar gain, and the NEC2 computer model and theoretical result get similar impedance.

From Figure 3.7 of the current distribution, we find that the current decreases gradually along the helix and it almost constant to a point near the end. We also find that the currents on the wires of the ground plane just below the bottom turn of the helix are very large.

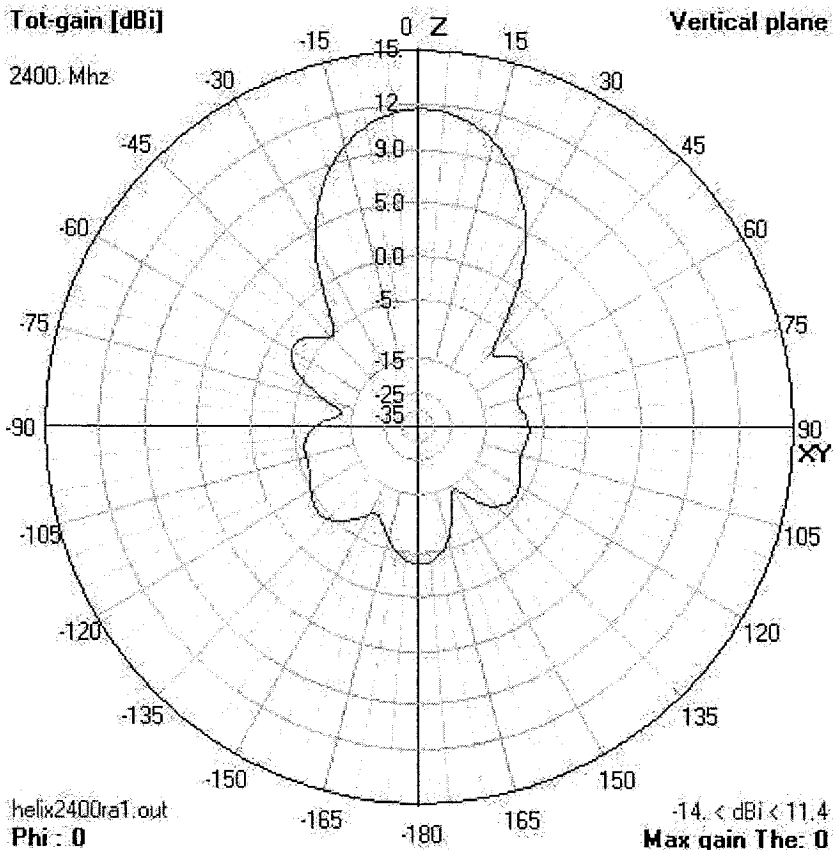

Figure 3.7 Radiation pattern of 2.4 GHz helix, computed from NEC2 model, gain on a dB scale.

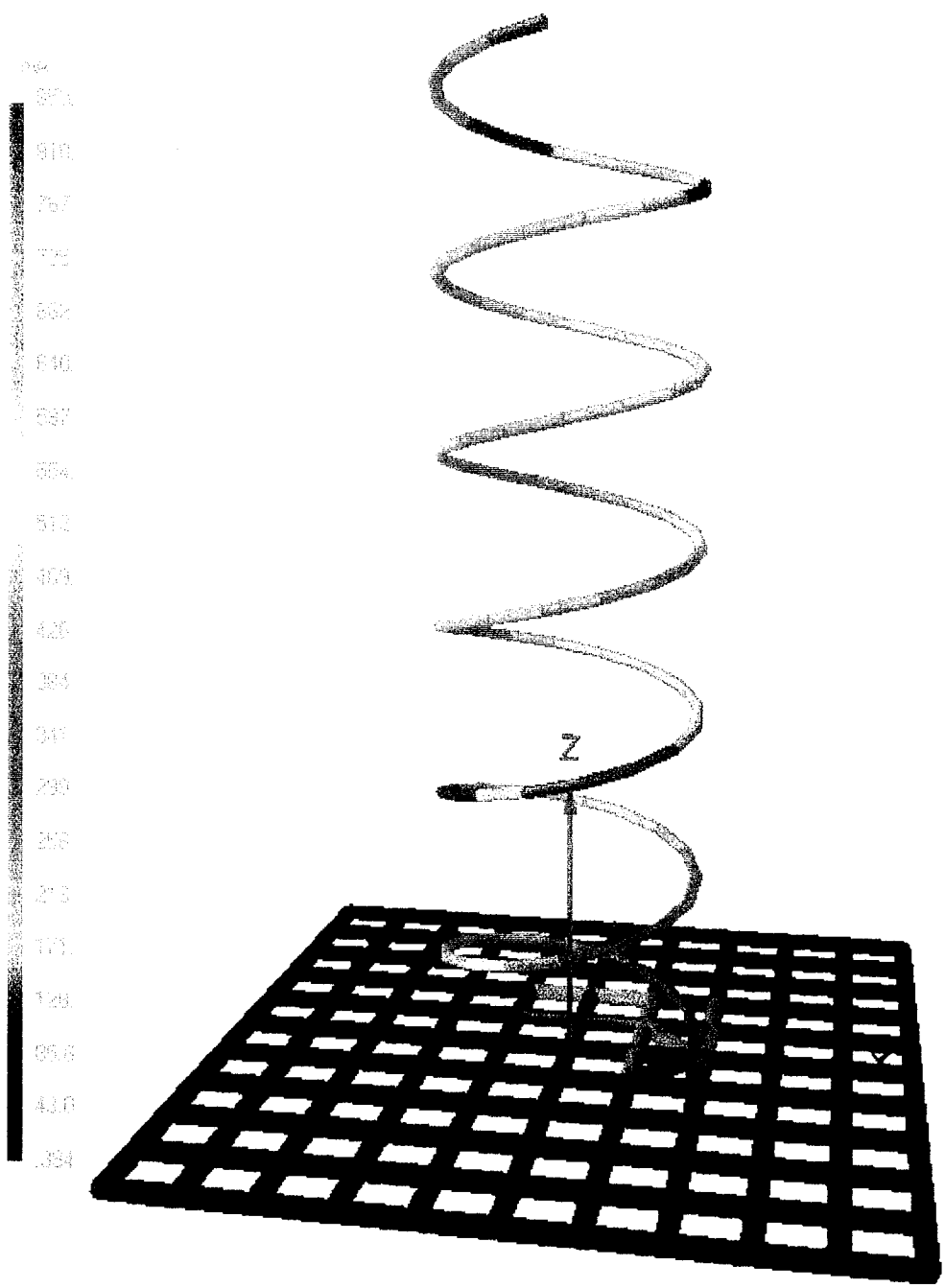

Figure 3.8 Current distribution on 2.4 GHz helix and ground plane.

3.2 Downlink Reflector Antenna

In practice, the whole process of manufacturing a single parabolic reflector can be very expensive, so a commercial Ku band satellite TV dish was used for the ground station.

3.2.1 Total Antenna Assembly

The dimensions for the Ku band offset parabolic antenna are $D = 76cm$, and $f/D = 0.59$. The manufacturer provided a support arm to install the feed. The process of measuring the reflector geometry to get the focus position and illumination angle of the reflector is given in Appendix A. Actually, we needed to adjust the feed position carefully to obtain the maximum gain in practice. The reflector with helix feed is shown in Figure 3.9.

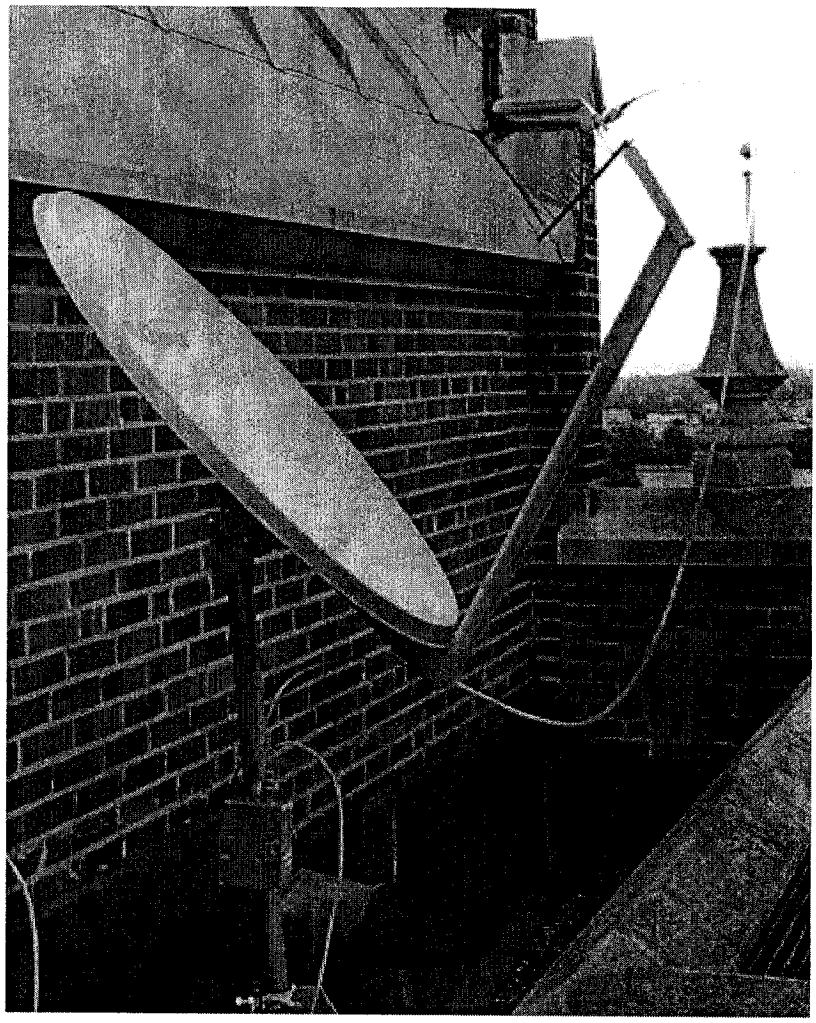

Figure 3.9 Installed reflector antenna with helix feed,

atop of the Loyola AD building.

3.2.2 Return Loss Measurement Results

After installing the helix feed on the reflector, the return loss of the feed was measured again. Figure 3.10 shows the result. Comparing with Figure 3.3, the reflector

has little effect on the antenna impedance. We see that the return loss is always better than 10 dB. Near the AO-40 beacon frequency of 2401.323 MHz, the return loss is about 15 dB.

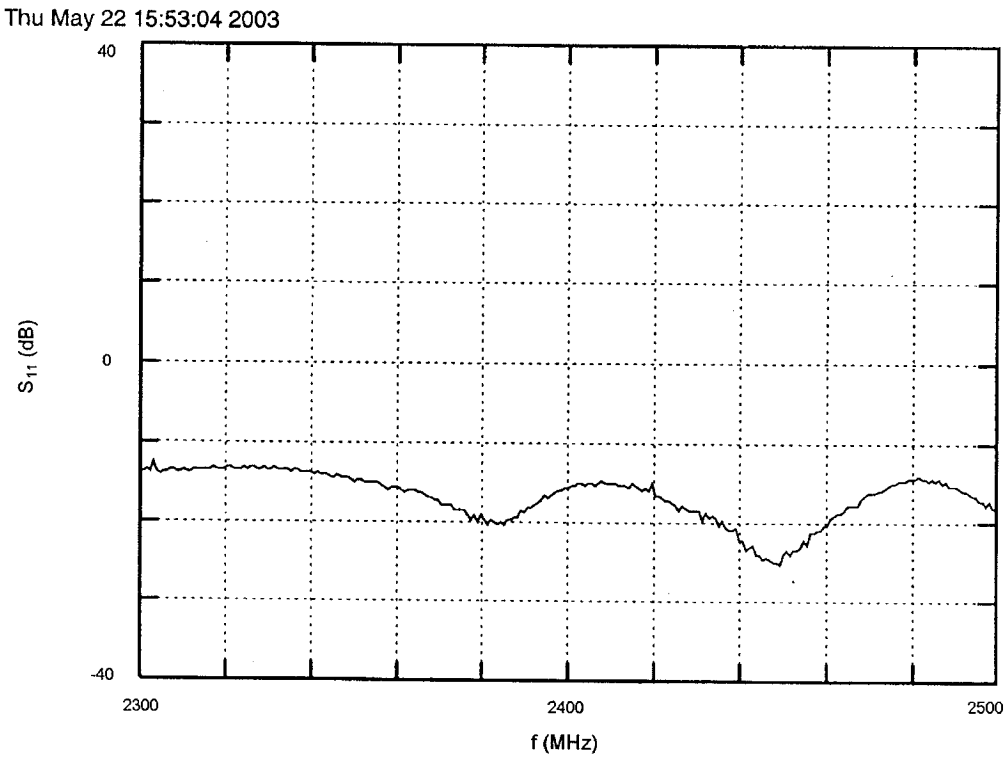

Figure 3.10 S_{11} of the feed with dish, 10 dB/div.

3.2.3 Pattern Measurement of the Dish

Using the same measurement system as was used for Figure 3.5, the gain of the parabolic reflector antenna is found to be approximately 18 dB by using the comparison method. The diameter of the dish is 76 cm, so the minimum distance to the far field is

about 10 meters, and this distance cannot be achieved in the lab. The largest possible distance between two antennas is only 6 meters and the height of the geometric center of the dish is 1.4 meters, for the experiment. Hence this measurement result is just regarded as approximate because of the uncertainty due to multipath effects. To get the accurate far field, it is required to bring the equipment outdoors. An even better option is to use the actual satellite as the transmitter source! By using prediction software, we know information about the satellite such as arrival of satellite time (AOS), loss of satellite time (LOS), azimuth, elevation, etc... Table 3.4 is the sample of the prediction result by using the software SatTrack[22]. It gives the information about the satellite AO-40, such as azimuth, elevation, height, squint angle ,etc... It also gives the Doppler shift frequency which should be adjusted on the receiver. According the result from the prediction software, we can select a suitable operating date and time to do the experiment. Then we were able to receive the signal from the satellite and measure the far field pattern for our antenna. Figure 3.11 shows the total receiving system of AO-40.

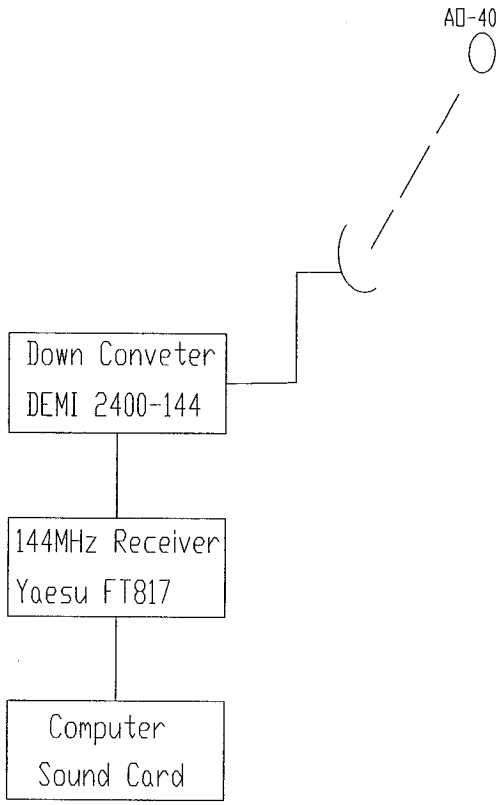

Figure 3.11 Receiver experiment, using signal from satellite.

The receiving system was set up as in Figure 3.11 and the elevation angle and azimuth of the dish was set according the prediction result. An azimuth angle of 0 degrees points North and 90 ° points East. An elevation angle of 0 ° points towards the horizon and 90 ° points towards the zenith. The antenna was set up in a wide-open space on the ground, near the HB building on the Loyola campus. The antenna was mounted on a pole in a tripod. A long screwdriver was put through a hole drilled in the pole, to serve as an azimuth angle pointer.

Table 3.4 Prediction result of AO-40 orbit.

STATION_ID SatTrack V3.1 Orbit Prediction

Satellite #26609 : AO-40 (AMSAT-AO40)
Data File : tlex.dat
Element Set Number: 341 (Orbit 1230)
Element Set Epoch : 04Jul03 22:54:47.313 UTC (39.8 days ago)
Orbit Geometry : 1023.76 km x 58803.86 km at 9.146 deg
Propagation Model : TLE Mean
Ground Station : Montreal, PQ, Canada --- FN35FM
Time Zone : EDT (-4.00 h)
Downlink Frequency: 2401.3230 MHz
Fri 15Aug03 --- Orbit 1283

EDT	Azimuth [deg]	Elev [deg]	Range [km]	Sun Ang [deg]	Doppler [kHz]	Loss [dB]	Squ Ang [deg]	Phs	Md	V
10:09:03	227.9	34.7	58334.7	99.8	+4.36	195.4	5.9	161	U/S	D
10:14:03	229.0	34.2	58168.2	100.1	+4.53	195.4	6.2	162	U/S	D
10:19:03	230.0	33.7	57995.3	100.4	+4.70	195.3	6.5	163	U/S	D
10:24:03	231.0	33.2	57815.8	100.6	+4.88	195.3	6.8	164	U/S	D
10:29:03	232.0	32.7	57629.8	100.9	+5.05	195.3	7.1	166	U/S	D
10:34:03	233.0	32.1	57437.1	101.1	+5.23	195.2	7.4	167	U/S	D
10:39:03	234.0	31.6	57237.7	101.4	+5.41	195.2	7.7	168	U/S	D
10:44:03	234.9	31.1	57031.5	101.7	+5.60	195.2	8.0	169	U/S	D
10:49:03	235.9	30.5	56818.4	101.9	+5.78	195.1	8.4	170	U/S	D
10:54:03	236.8	30.0	56598.3	102.2	+5.97	195.1	8.7	171	U/S	D
10:59:03	237.7	29.4	56371.1	102.5	+6.16	195.1	9.0	172	U/S	D
11:04:03	238.6	28.9	56136.8	102.8	+6.35	195.0	9.4	173	U/S	D
11:09:03	239.5	28.3	55895.3	103.1	+6.55	195.0	9.7	175	U/S	D
11:14:03	240.4	27.7	55646.4	103.4	+6.74	195.0	10.1	176	U/S	D
11:19:03	241.3	27.2	55390.0	103.6	+6.94	194.9	10.5	177	U/S	D

We set the reference azimuth angle for maximum signal strength firstly, and then changed the azimuth clockwise and anticlockwise, to obtain the pattern of the antenna. Table 3.5 shows the data for this experiment. The antenna pattern data was obtained by receiving the AO-40 telemetry beacon, which transmits at 2401.323 MHz. The power levels were recorded on the receiver signal strength meter (the S meter). Measurement was also attempted on the roof of the AD building, but it was decided there is no advantage to that location.

Table 3.5 Received data for the dish, using the 2401.323 MHz beacon.

Signal strength	Theoretical IF Signal power(dBm)	Azimuth(°)
S8	-79	0
S7	-85	5.5
S6	-91	12.6
S5	-97	16
S4	-103	18
S3	-109	19.5
S2	-115	20.5
S1	-121	22

3.2.4 Measurement data processing

We did some additional experiments to calibrate the receiver, and made some theoretical derivations to get the relationship between the directivity and the N-dB beamwidth we measured. Then we were able to obtain the gain and the pattern, from the measurement results.

3.2.4.1 Calibration of the Receiver

A Yaesu FT817 amateur radio transceiver was used as the receiver. It has an S-meter for displaying the received signal strength. In theory, a receiver S meter is calibrated so that a reading of S9 corresponds to 50 uV across a 50 ohm load, or -73 dBm. A drop in one S-unit represents 6 dB, so S8=-79 dBm, and so on. In practice, the power readings taken with this might not be that accurate. The S-meter accuracy was checked against a precision RF generator, the HP E3348C, and correction factors were obtained. The corrected values are also shown in Table 3.6. The step of the S meter of a receiver is 6 dB in theory. We found that the S-meter was very inaccurate, and had to correct the measured readings. To calibrate the receiver, we used an HP E4438C signal generator to generate power levels on the order of -120 dBm, similar to our received signal. The signal generator has a readout which gives the power in dBm. Figure 3.12 shows the calibration setup, and Table 3.6 shows the calibration results.

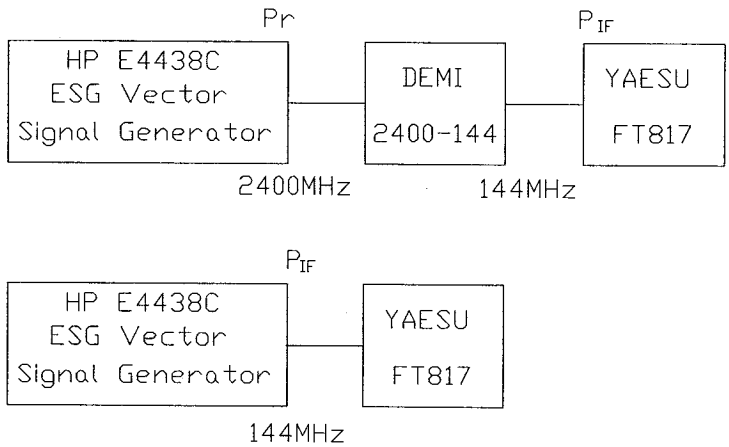

Figure 3.12 Receiver calibration setup.

Table 3.6 Received data of the dish with calibration.

Signal display on FT817	P_{IF} (dBm)	P_r (dBm) on HP E4438C	Normalization (dB)	Azimuth angle(°)
S8	-104	-128	0	0
S7	-106	-130	2	5.5
S6	-107	-131	3	12.6
S5	-108	-132	4	16
S4	-109	-133	5	18
S3	-110	-134	6	19.5
S2	-111	-135	7	20.5
S1	-112	-136	8	22

The pattern data in Table 3.6 was collected in the following way. The antenna azimuth and elevation were adjusted for maximum, which was S8. By slightly rotating the antenna in azimuth by 5.5 °, the meter dropped to S7. In theory, S8 to S7 is a 6 dB drop. In practice, because of the meters inaccuracy, it was a change from -128 dBm to -130 dBm, or a 2dB drop. Continued rotation in azimuth, and taking of S meter readings allowed us to obtain the antenna pattern. By applying correction factors to the S meter readings, we believe that the final result for the measured radiation pattern is accurate.

3.2.4.2 Gain Obtained from Measurement Result

In this section we will find the gain from the measured pattern data. We know that the pattern of the uniform distribution for circular apertures has the form of[23]

$$f(k_r) = \left| \frac{2J_1(ka\sin\theta)}{ka\sin\theta} \right|. \tag{3-4}$$

We define the N-dB pattern point as the point on the radiation pattern where the level has dropped by N dB, relative to the main beam maximum. We get the N-dB pattern point from (3-4), thus we can obtain the value of $\sin\theta$. Since

$$ka\sin\theta = \frac{2\pi}{\lambda}\frac{D}{2}\sin\theta = \frac{\pi D}{\lambda}\sin\theta = c \tag{3-5}$$

we have

$$\theta = \arcsin\frac{c}{\pi D/\lambda} \quad . \tag{3-6}$$

For large apertures, we can approximate $\sin\theta$ by $\theta(rad)$. Therefore, we can get that the N-dB beamwidth is

$$N_{dB}BW = \frac{2c}{\pi D/\lambda}(rad), \tag{3-7}$$

so the directivity D and beamwidth BW are related by

$$\frac{\pi D}{\lambda} = \frac{2c}{N_{dB}BW(rad)}. \tag{3-8}$$

on the other hand, the directivity of a circular aperture is[24]

$$D_0 = (\frac{C}{\lambda})^2 = (\frac{\pi D}{\lambda})^2. \tag{3-9}$$

Hence, we have

$$D_0 = (\frac{2c}{N_{dB}BW(rad)})^2 = 13131(\frac{c}{N_{dB}BW(\deg)})^2. \tag{3-10}$$

We can use the 3 dB, 10 dB as any value N dB of beamwidth to estimate the antenna directivity from (3-10). Using the data from Table 3.6, the gain of the dish is calculated in Table3.7.

Table 3.7 Gain of the reflector with helix feed.

N dB	$f(k_r)$	$ka\sin\theta = c$	$N_{dB}BW(^o)$	Directivity(dB)
3dB	0.707	1.62	12.6	23.4
4dB	0.631	1.88	16	22.6
5dB	0.562	2.08	18	22.4
6dB	0.501	2.25	19.5	22.4
7dB	0.447	2.35	20.5	22.4
8dB	0.339	2.49	22	22.3

From the measured beamwidth data, we can draw the conclusion that the gain of the dish is about 22dB. From (2-39), we also have the theoretical result

$$G_e = \varepsilon_{ap}(\frac{\pi D}{\lambda})^2 = 0.55\times(\frac{\pi\times 76}{12.5})^2 = 23dB\,.$$

It is seen that these two results are in good agreement.

3.2.5 Computer Model of the Reflector Antenna

C. J. Sletten's software[25] REF.FOR was used to calculate the gain and pattern of this parabolic antenna. It computes the far field of the offset parabola by the aperture field integration method. The software calculates the far field pattern of the reflector by using the geometry of the parabola and the pattern of the feed. Appendix G gives the input file for REF.FOR. The feed pattern was obtained from the result of the helix feed NEC code

simulation output file. Appendix H shows the output data. The gain of the dish is 22.7 dB from the simulation result. This value equals the result from Section 3.2.4.2. Figure 3.13 plots the theoretical and experimental pattern of the dish. The beamwidth data we got are insufficient because of the limited of the receiver S meter, but from Figure 3.13, we still can find that the error of beamwidth is less that 10%.

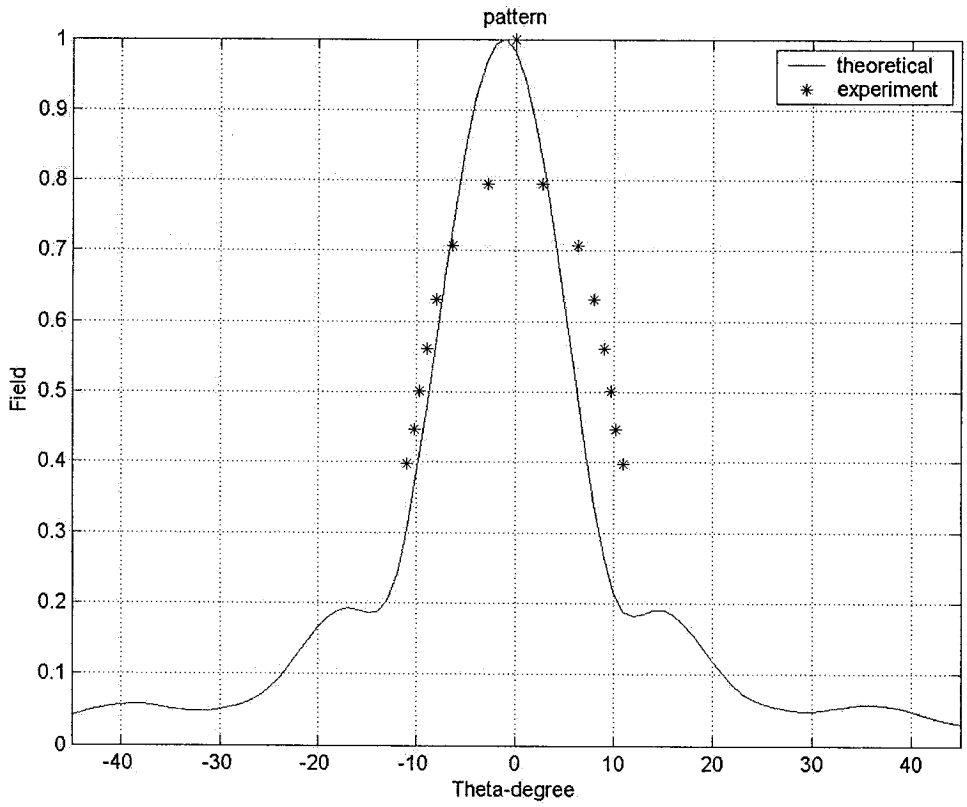

Figure 3.13 Theoretical and experimental radiation pattern of the reflector with helix feed, E_θ on a linear scale.

3.3 Reception of Satellite Signal

Using the system in Figure 3.11, and connecting the output of the receiver to the sound card of a computer, the beacon's telemetry signal and the operating status of the satellite was obtained.

The reflector feed is connected to a down converter, which changes the received 2.4 GHz signal into 144 MHz. The down converter is a DEMI 2400-144, manufactured by Down East Microwave, Inc., USA. The exact operating frequency during the test was 2401.323 MHz. The down converted signal is fed into the Yaesu FT-817 receiver for the 2 meter band, tuned to 145.328 MHz. The received signal is Doppler shifted to 145.347 MHz because of the satellite motion. At the audio output, a BPSK signal is present. Feeding this into the soundcard input of a computer and using the software AO40RCV[26], we can decode the satellite telemetry. Typical results are shown in Figure 3.14 and Figure 3.15. The data contains information on the satellite orbit and other aspects.

In summary, the experiment was success and we received and decoded the satellite signal.

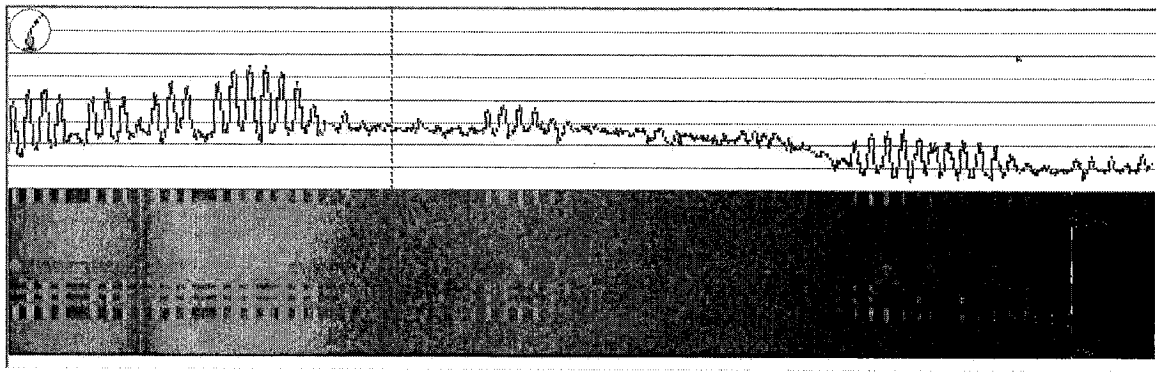

Figure 3.14 Telemetry audio signal and spectrum received from AO-40.

```
+=+=+=+=+=+=+=+=+=+=+=+=  M A I N    S T A T U S  +=+=+=+=+=+=+=+=+=+=+=+

A  HI, THIS IS AMSAT OSCAR-40        2003-08-15  14:17:46  #0A75
+-------------------------------------------------------------------------+
|  Hgt: 55240 km   Lon: -110  Lat: 5   ALON: 2  ALAT: 2                   |
+-------------------------------------------------------------------------+

AMSAT Day = 9357    Orbit# = 1281   MA = 164
Current AMSAT Day = 9558
---------------------  R E C E I V E R S ----------------------------
21MHz: OFF        24MHz: OFF        V: Off           U: On HiGain
L1:  HiGain       L2: ON            S1: OFF
S2: OFF           C: OFF            Leila: #92D8
-------------------  T R A N S M I T E R S ------------------------
U: Off        V: Off        S1: OFF        S2: ON
X: Off        K: Off
-----------------------  A G C / A L C ------------------------------
V-Rx: -12.77dB        U-Rx: 8.32 dB       L1-Rx: 0.61 dB
L2-Rx: -0.28dB        S1-Rx: -62.14dB     S2/C-Rx: -253.70dB
HF-Rx: 008       V-Tx: 084      U-Tx: 008      S2-Tx: 077
-----------------------  B E A C O N S ------------------------------
CB: ON        CB FSK: OFF       DPSK: ON        EB: OFF
```

Figure 3.15 Decoded telemetry information from AO-40.

Chapter 4

Uplink Antenna Design and Testing

4.1 Uplink Helix Antenna Design

At UHF, we also can use a helix antenna for the uplink at 435MHz. Since this antenna must transmit the signal to the high orbit satellite, gain is the major factor we should consider. Using the same procedure as in the design of the 2.4 GHz helix, the dimensions of UHF antenna are given in Table 4.1.

Table 4.1 Geometric dimension of 435 MHz uplink helix[27].

Parameter		Ratio vs. wavelength
Turns N	13	---
Wavelength λ	69 cm	---
Diameter of each turn D	20.8 cm	---
Space of each turn S	15.2 cm	0.22λ
Circumference C	65.3 cm	0.95λ
Ground plane side length G	70 cm	λ
Pitch angle α	13^0	---

4.2 435 MHz Helix Assembly

Because of the big dimension of this helix, we had to use 3/4" wood poles to support the whole helix antenna. The following materials were needed: one 70 cm by 70 cm aluminum sheet, 25 feet 1/4" copper pipe for the helix, and some copper foil to make a 1/4 turn matching section. To make the helix, these steps are followed:

(A) Drill the ground plane, install the N connector.

(B) Trim the copper foil, the width of the foil is about 4 cm.

(C) Wind the copper pipe right hand circular polarized RHCP.

(D) Use a high power soldering iron to solder the matching turn.

(E) Fix the helix to the wood frame.

(F) Install the N connector on the ground plane.

(G) Solder the helix, being careful with the distance between the last turn of the helix and the ground plane.

4.3 Measurement Results

This section gives the return loss measurement result for the 10:1 scale model helix of the UHF antenna and the result for the full size UHF helix.

4.3.1 Scale Model

Because of the large size of the antenna, it was hard to make adjustments and measurements in the lab. A 10:1 scale model was made to measure the performance of the antenna. Figure 4.1 shows the UHF antenna and the scale antenna. That means, everything was scaled by 1/10, and the operation frequency is 4.35 GHz. The measured return loss of this scale model is shown in Figure 4.2. From Figure 4.2, the return loss of the 4.35 GHz antenna is seen to be extremely good. Using the comparison method and an ECO3115 horn, the gain of the 4.35 GHz antenna was found to be about 13 dB. That means the gain of the full size 435 MHz antenna should be also 13 dB.

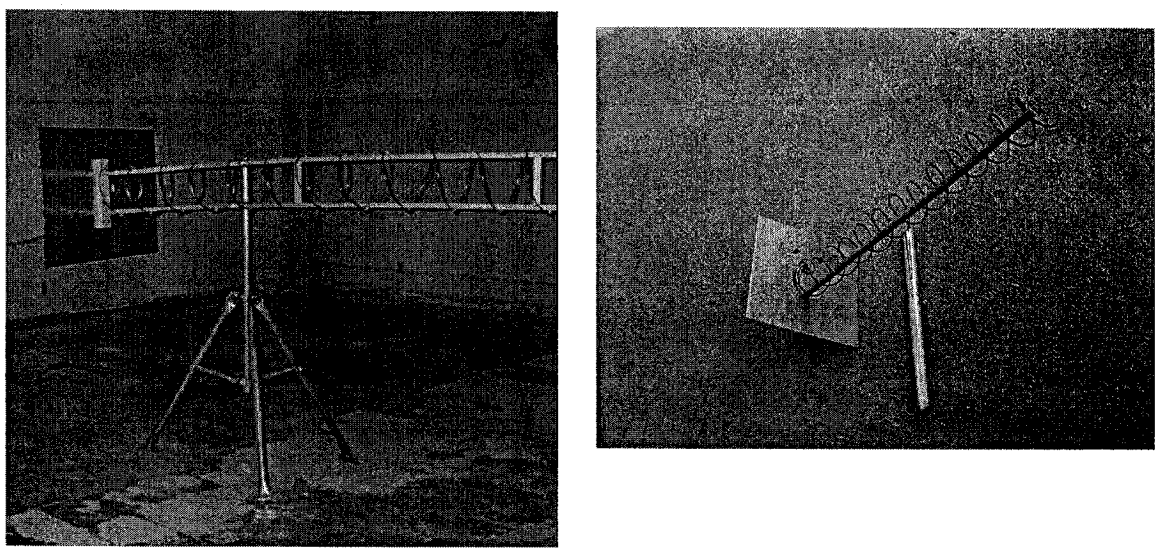

Figure 4.1 435 MHz helix antenna and 4350 MHz helix antenna, left: 435 MHz helix; right 4350 MHz helix. The boom length of the 435 MHz helix is 2 meter and it is 20 cm for the 4350 MHz helix.

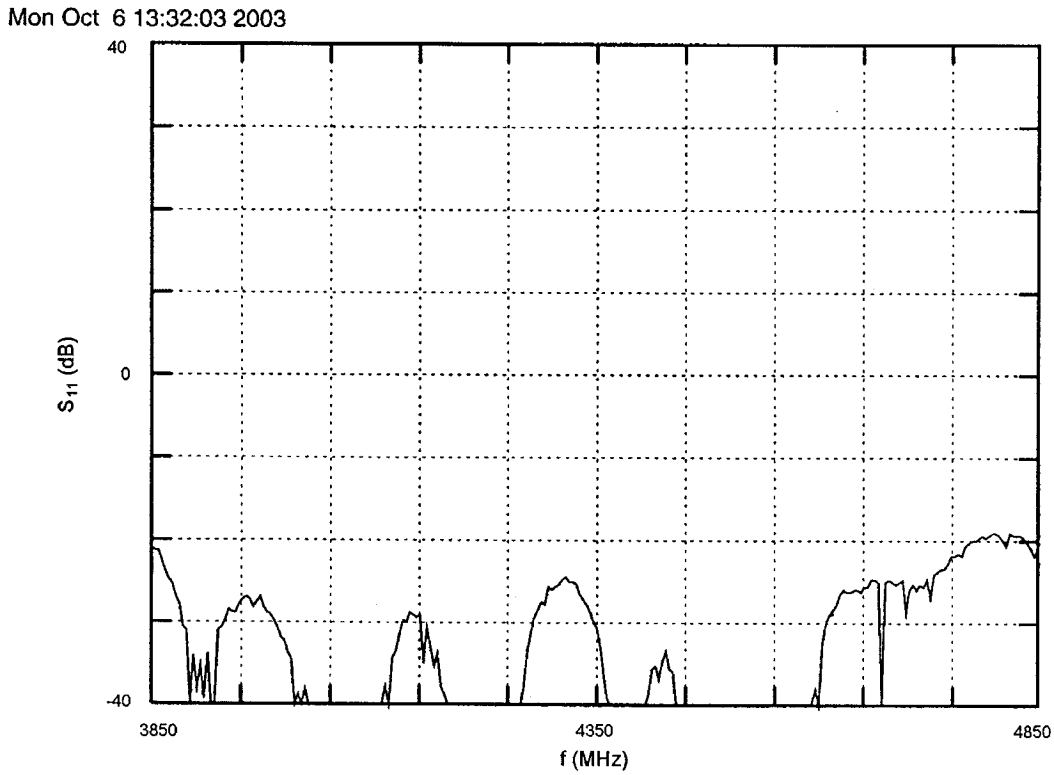

Figure 4.2 S_{11} of 4.35 GHz scale model helix antenna, 10 dB/div.

4.3.2 Return Loss of 435 MHz Antenna

It was possible to measure the RL of the 435 MHz antenna, in a large space that was temporarily available in the former location of the Physics department. An HP 8505 network analyzer was used. It can measure impedance from 500 KHz to 1.3 GHz, and was able to cover our frequency range of interest. Figure 4.3 shows the measurement system to measure the VSWR of the 435 MHz antenna.

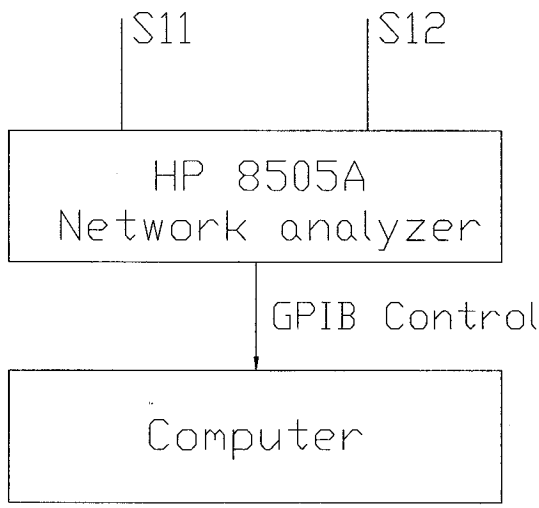

Figure 4.3 435 MHz helix S_{11} measurement system.

Comparing Figure 4.2 and Figure 4.4, it is seen that the result of RL of 435 MHz is not as good as the scale model, because it is hard to make a accurate scale structure to high precision. But the RL is still good enough, and it is better than 20 dB at 435 MHz.

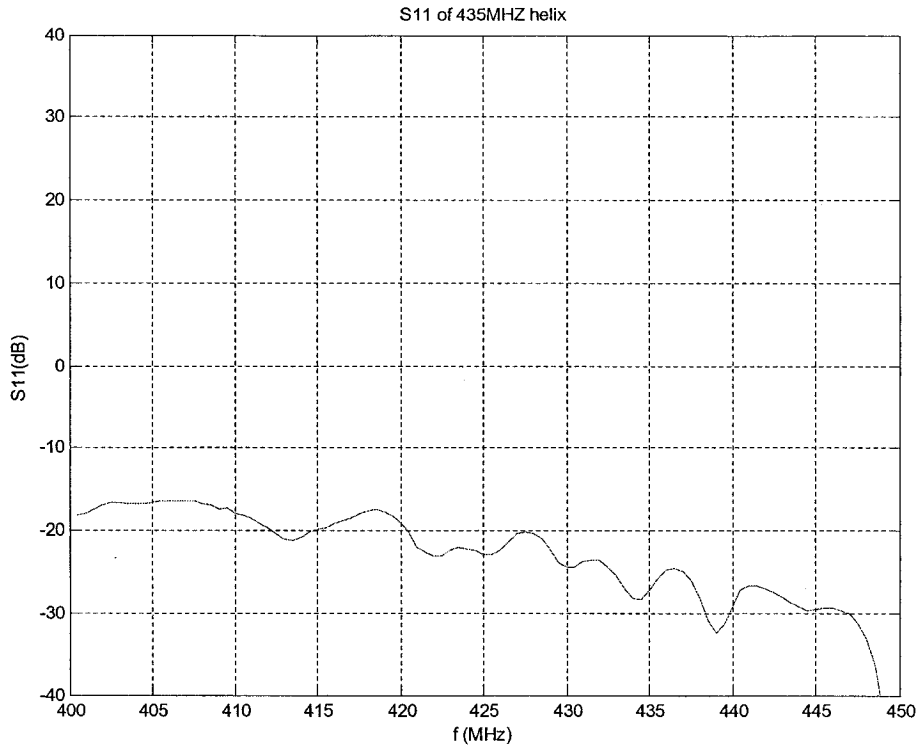

Figure 4.4 S_{11} measured result for the full size 435 MHz helix.

4.4 Computer Model of UHF Uplink Antenna

This section describes the computer model for the reflection coefficient of the UHF helix with the matching section, and gives the NEC model for the UHF helix antenna.

4.4.1 Reflection Coefficient with Transformer

In Chapter 3, we were able to use an approximate model to calculate the reflection coefficient of a helical antenna's matching network. We now follow the same procedures

again, except using new dimension for the 435 MHz design. Here W=40mm, and d=5mm~22mm[28], the total length of the 1/4 turn arc is about 163mm. Figure 4.5 shows the calculation result. It is assumed that the transformer is matching a 50Ω line to a 130Ω load (the antenna). A 9 dB return loss represents a slight improvement over the 7 dB that would be obtained with no matching network. However the approximate model did not predict results as good as for the 2.4 GHz helix feed in Chapter 3. Furthermore, the measured return loss is much better than the model's prediction, indicating that this model is inadequate.

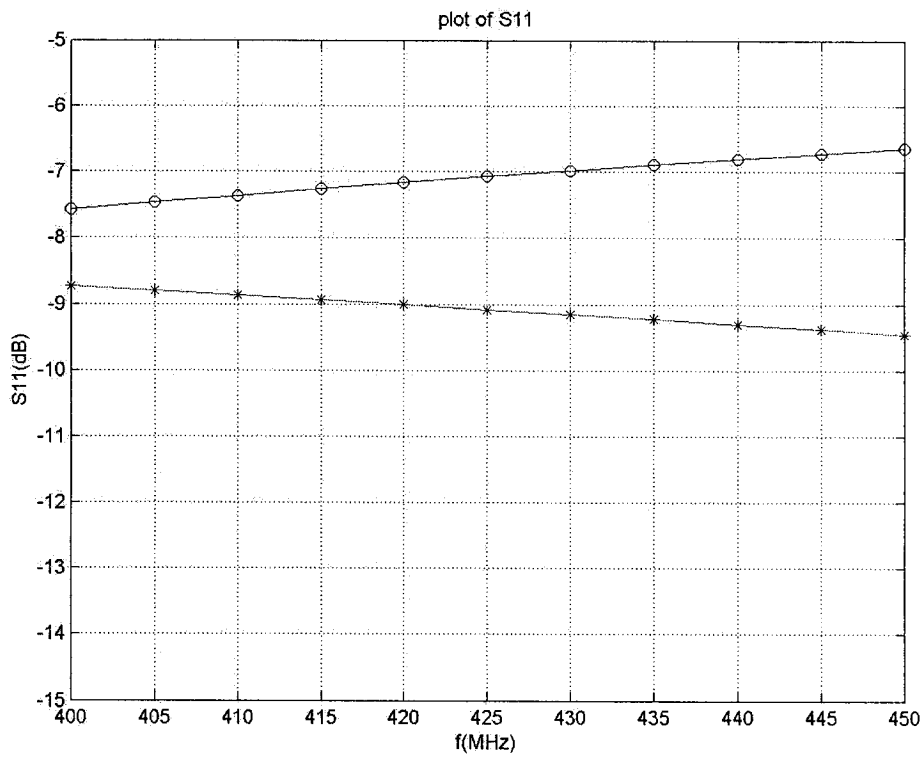

Figure 4.5 Theoretical S_{11} of 435 MHz helix antenna.

* S_{11} with matching network, ∘ S_{11} without matching.

4.4.2 Radiation Pattern

After modeling the 435 MHz helix with NEC2, we obtained the simulation results. Table 4.2 is the comparison results of the NEC model and the theoretical calculations. Appendix D and Appendix F show the 435 MHZ helix antenna input file and output file for the NEC2 model respectively. Figure 4.6 is the pattern of 435 MHz helix antenna. Figure 4.7 is the current distribution in this helix.

In summary, the 435 MHz helix with matching network gave us a measured return loss of better than 20 dB. The scale model's measured gain of 13 dB was in good agreement with the NEC model's result of 12.4 dB. The matching network model, using a taped transmission line, was not very accurate. The directivity of 16 dB predicted by the helix design formula was less accurate.

The currents are strongest in the immediate vicinity of the feed region.

Table 4.2 Comparison of resultsfor the 435 MHz helix.

	HPBW(^{0})	Gain(dB)	Impedance(Ω)	RL(dB)
Scale mode measurement	---	13	---	30
NEC2 model	40	12.4	90.4-j77	---
(2-11)-(2-14) calculation	32	16	133+j0	7
Full size measurement	----	----	---	25

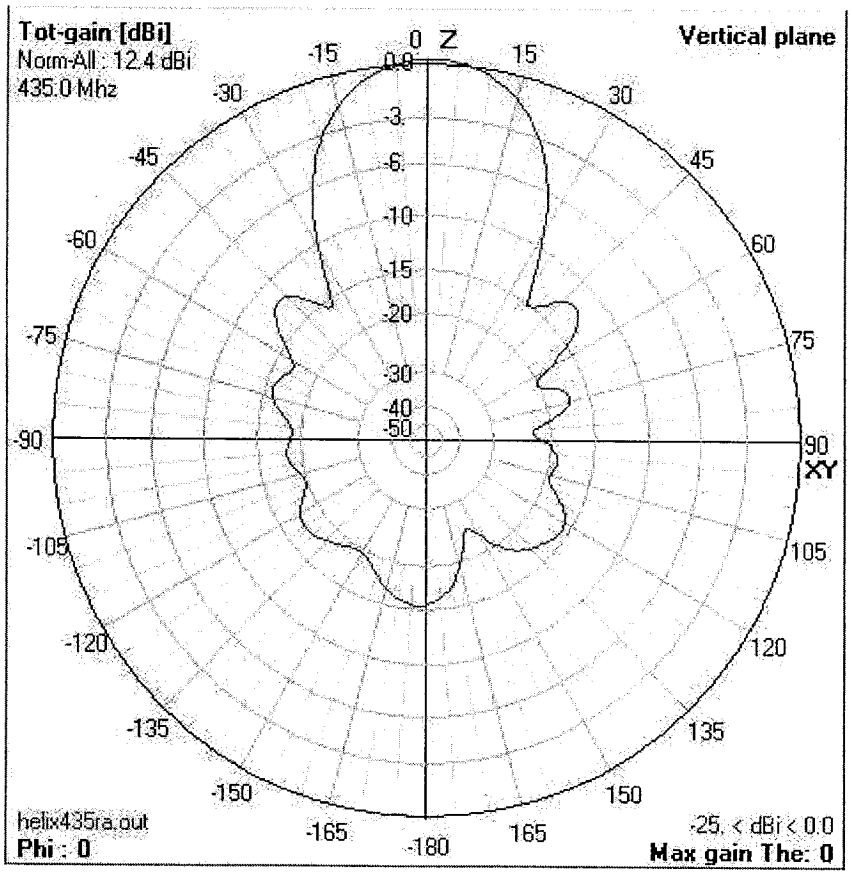

Figure 4.6 Radiation pattern of 435 MHz helix, using NEC2 model,

Gain on dB scale.

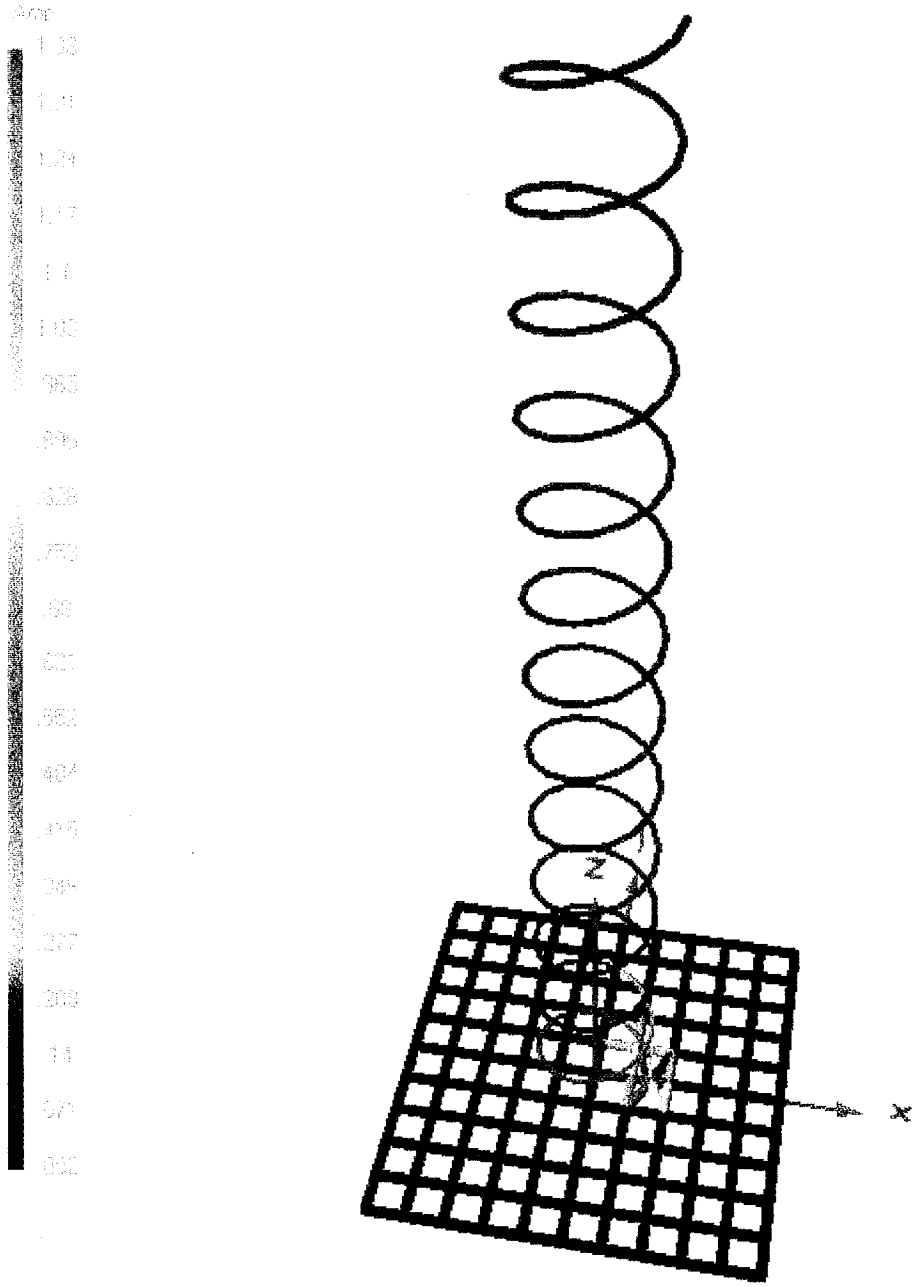

Figure 4.7 Current distribution in 435 MHz helix, using NEC2 model.

Chapter 5

Conclusion

In this thesis we designed, modeled, and tested the downlink and uplink antennas to the used in amateur radio satellite communication.

In Chapter 2, we discussed the background theory of antennas, and also talked about the numerical technique Method of Moments and the NEC2 code, which is used to model the antenna.

In Chapter 3, we gave the design and assembly process of the helix feed antenna in detail. A method was given to analyze the matching structure of the helix antenna and obtained the wire grid model simulation result of a helix antenna by NEC2. The NEC model is quite good for computing radiation pattern of a helix antenna. One could also develop the helix model with matching network using NEC, in future research. We also gave the experimental results of the helix feed and whole downlink antenna. The downlink antenna achieves the performance of RL>15 dB, and Gain=22 dB. After assembling the total downlink system, we received and decoded the AO-40 satellite telemetry signal.

In Chapter 4, a 435 MHz helix antenna was designed for the uplink. A 10:1 scale model was used to measure the gain, because adequate space was not available to test the full-size UHF antenna. The measured gain of the scale mode was in good agreement with

the NEC model. The UHF scale model achieves RL>20 dB and Gain=13 dB. The trial computer model of matching section for this UHF band is inadequate, and it should be supplemented and modified in further research.

It is noted that there have been hardware problems with the satellite AO-40 after January 2004, and the uplink experiment could not be finished. This task should be continued if AO-40 gets repaired.

Some people present a modified helical structure — tapered several turns of the helix at the open circuit end — to improve the axial ration performance of the helix antenna[29]-[31]. This also could be verified in a future experiment.

The total cost of these antennas is less than CDN $150, so it is clear that amateur radio satellite communications are achievable at low cost.

References

[1] AO-40 FAQ, *Available: http://www.amsat.org* [online].

[2] M. Davidoff, *The radio amateur's satellite handbook.* ARRL, Newington CT, 1998.

[3] H. Long, "Entry Level AO-40 Capable Satellite Stations," 16th AMSAT-UK Colloquium, Guildford, England, July 27-29 2001.

[4] H. Long, "A Quadruple Helix for AO-40," *Available: http://www.g6lvb.com* [online].

[5] C.A. Balanis, *Antenna Theory, Analysis and Design.* New York: Wiley, 1982, Chapter 2, Chapter 16.

[6] C. W. Trueman, Unpublished class notes, Concordia University.

[7] C.G. Montgomery, *Technique of Microwave Measurements.* Boston Technical Publishers, 1964.

[8] J. D. Kraus, *Antennas for All Applications.* New York: McGraw-Hill, 2002.

[9] *The Antenna Handbook*. ARRL, Newington CT, 1997.

[10] R.F. Harrington, *Field Computations by Moment Methods*. New York: Macmillan, 1968.

[11] G. J. Burke and A. J. Poggio, "Numerical Electromagnetic Code (NEC) - Method of Moments," Naval Ocean Syst. Center, San Diego, CA, *NOSC Tech. Document 116*, Jan. 1981.

[12] C.W. Trueman & S.J. Kubina, "Verifying wire-grid model integrity with program 'check' ," *ACES Journal*, Vol.5, No.2, p.17-42, 1990.

[13] W. L. Stutzman and G. A. Thiele, *Antenna Theory and Design*. New York: Wiley, 1981, p.268

[14] *ibid*, p. 265-267.

[15] J.D. Kraus, "A 50-Ohm input impedance for helical beam antennas," *IEEE Trans on AP*, Vol. 25, No.6, p.913, June 1977.

[16] D. M. Pozar, *Microwave Engineering*. New York: Wiley, 1998, Chapter 5.

[17] A.W. Love, *Reflector Antennas*. New York: IEEE Press, 1978.

[18] R. C. Johnson, *Antenna Engineering Handbook*. New York: McGraw-Hill, 1993.

[19] B. Zauhar, "Modified 80cm Offset Dish for 2.4GHz Reception," *Available: http://www3.sympatico.ca/b.zauhar* [online].

[20] H. Long, "Modify an analogue sky TV offset fed dish for AO-40 S-band," *Available: http://www.g6lvb.com* [online].

[21] D. M. Pozar, *Microwave Engineerin*. New York: Wiley, 1998, p. 162.

[22] M. Bester, "SatTrack V3.1," software available from ftp://ftp.amsat.org/amsat/software/Linux/ [online].

[23] T.A. Milligan, *Modern Antenna Design Design*. New York: McGraw-Hill,1985, p. 159.

[24] C.A. Balanis, *Antenna Theory, Analysis and Design*. New York: Wiley, 1982, p.484.

[25] C. J. Sletten , *Reflector and Lens Antenna Design*. Artech House, 1988.

[26] M. Wheatley, "AO40RCV V1.4," software available from http://www.qsl.net/ae4jy/ao40rcv.htm [online].

[27] B. Zauhar, "435MHz 12-turn Helix Antenna," *Available: http://www3.sympatico.ca/b.zauhar/* [online].

[28] 435MHz 9-turn Helix, *Available: http://www.ntay.com/helix* [online].

[29] U. R. Kraft, "Main Beam Polarization Properties of Modified Helical Antenns," *TEEE Trans on AP*, Vol.38, No.5, pp.589-597, 1990.

[30] C. Donn, "A New Helical Antenna Deign for Better On and Off Boresight Axial Ratio Performance," *TEEE Trans on AP*, Vol.28, No.2, pp.264-267, 1980.

[31] Michael Slater, "An Innovative Antenna Design Tool: The Antenna Design Software," Concordia University Thesis (M.A.Sc.), 2001.

Appendix A

Reflector Antenna Geometry

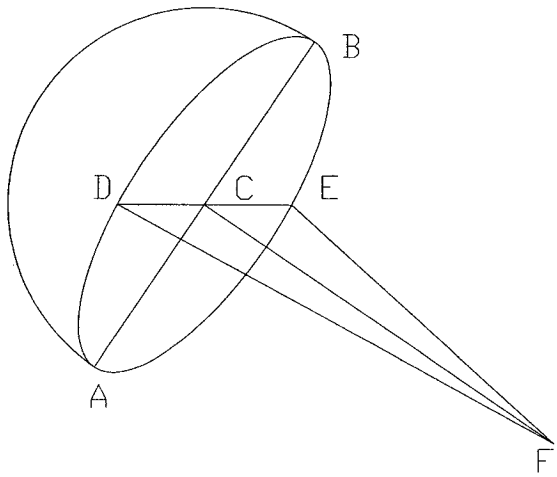

Figure A-1. 3D Geometry for the offset parabolic reflector aperture.

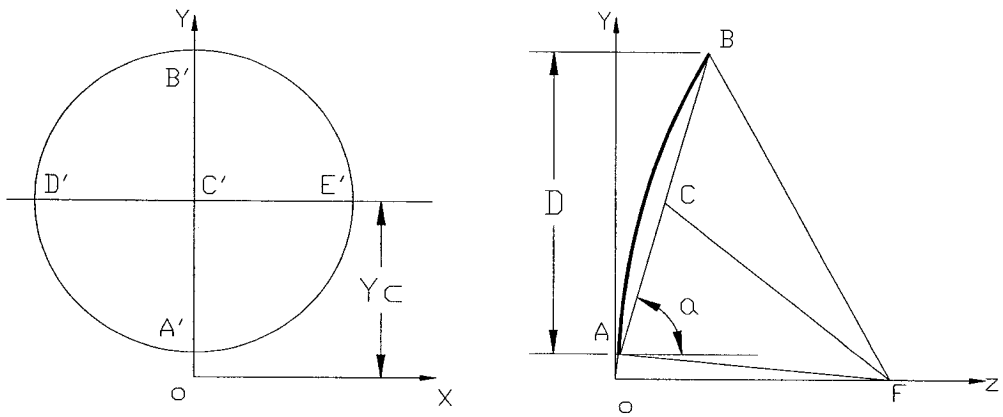

Figure A-2. Front view and side view for the offset parabolic reflector.

Figure A-1 and Figure A-2 show the geometry for the offset reflector. AB is the long axis

of the aperture ellipse; CD is the short axis of the aperture ellipse; C is the center of the aperture; D is the diameter of the projected aperture; YC is the offset of the center.

The manufacturer provides some parameters of the dish:

effective aperture $D = 76cm$

focal distance $f = 44.6cm$

$f/D = 0.59$

long axis of the ellipse $AB = 83cm$.

So

tilt angle $a = \sin^{-1}\frac{AB}{A'B'} = \sin^{-1}\frac{76}{83} = 66.3°$.

Assume the coordinate of A is (y,z),

then B is $(y+76, z+83\cos 66.3°)$, C is $(y+\frac{76}{2}, z+\frac{83}{2}\cos 66.3°)$.

We know, $x^2 + y^2 = 4fz$, and at the plane yoz, $x = 0$.

Hence

$$\begin{cases} y^2 = 4\times 44.6\times z \\ (y+76)^2 = 4\times 44.6\times (z+33.36). \end{cases}$$

Solving this equation, we have

$$\begin{cases} y = 1.154cm \\ z = 0.0075cm, \end{cases}$$

so the offset of the center $YC = 39.154cm$.

The coordinate of the focus F is (0,44.6) cm.

The distance $FC = \sqrt{y_c^{\ 2} + (44.6 - z_c)^2} = 48.08cm$.

Since $D'E'$ is the projection of DE, and $D'E' = DE$, hence $DE // D'E''$

$\because D'E' \perp A'B'$

$\therefore DE \perp A'B'$

and $DE \perp AB$

hence $DE \perp AA'BB'$,

i.e. DE is perpendicular to the plane yoz

so that $DE \perp FC$

$\because DC = CE = 38cm$

$\therefore \angle DFC = \tan^{-1}\dfrac{DC}{FC} = 38.3°$.

The illumination angle of the reflector is hence $2 \times 38.3 = 77°$.

Appendix B

Gain for Double Ridged Guide Antenna EMCO 3115

Gain and Antenna Factors for Double Ridged Guide Antenna
Manufactured by EMC Test Systems, LP
Model Number: 3115 Serial Number: 6793
1.0 Meter Calibration Polarization: Horizontal

Frequency (MHz)	Antenna Factor (dB/m)	Gain Numeric	Gain dBi
1000	24.2	3.99	6.0
1500	25.5	6.68	8.2
2000	27.8	7.03	8.5
2500	28.8	8.74	9.4
3000	30.7	8.07	9.1
3500	31.9	8.28	9.2
4000	33.1	8.32	9.2
4500	32.8	11.12	10.5
5000	34.0	10.41	10.2
5500	34.7	10.72	10.3
6000	35.0	11.86	10.7
6500	35.1	13.75	11.4
7000	36.3	12.04	10.8
7500	37.3	11.09	10.4
8000	37.3	12.41	10.9
8500	37.9	12.23	10.9
9000	38.1	13.09	11.2
9500	38.0	14.87	11.7
10000	38.5	14.96	11.7
10500	38.6	16.06	12.1
11000	38.6	17.66	12.5
11500	39.5	15.75	12.0
12000	39.3	17.69	12.5
12500	39.4	18.84	12.8
13000	40.8	14.86	11.7
13500	41.3	14.16	11.5
14000	42.2	12.29	10.9
14500	41.9	14.19	11.5
15000	40.4	21.68	13.4
15500	39.4	28.87	14.6
16000	40.1	26.35	14.2
16500	41.1	21.94	13.4
17000	42.4	17.44	12.4
17500	46.1	7.85	9.0
18000	47.9	5.53	7.4

Specification compliance testing factor (1.0 meter spacing) to be added to receiver meter reading in dBV to convert to field intensity in dBV/meter. Calibrated 12 Apr 02 (DD/MM/YYYY). Calibration per ARP 958.

Appendix C

NEC Input File for 2.4 GHz Helix

```
CM 2400MHz HELIX N=5.75 D=2.3CM S=3CM HEIGHT ON PLANE IS 3mm
CM FC is 2400MHz WL=12.5cm wire radius is 1.1mm
CM USE 1 WAVELENGTH PLANE GRID BY 0.1WL SO WR=WL/22PI=0.181CM
CM LH=5.75S=17.25CM
CM sweep freq. from 2300MHz to 2500MHz
CM  5   10   15   20        30        40        50        60        70        80
CM  v    v    v    v         v         v         v         v         v         v
CM----_____-----_____----------_________----------_________----------_________
CE
SY  F=2400
SY  LH=.1725
SY  L=0.125
SY  D=0.023
SY  R=.0011
SY  WR=0.00181
SY  S=0.03
SY  H=0.003
GH988   90        S        LH        D         D         D         D         R
GM988    0        0         0        0         0         0         H
GW101   10      -L/2      -L/2        0       L/2      -L/2         0        WR
GW102   10      -L/2      -2L/5       0       L/2      -2L/5        0        WR
GW103   10      -L/2      -3L/10      0       L/2      -3L/10       0        WR
GW104   10      -L/2      -L/5        0       L/2      -L/5         0        WR
GW105   10      -L/2      -L/10       0       L/2      -L/10        0        WR
GW106   10      -L/2        0         0       L/2        0          0        WR
GW107   10      -L/2       L/10       0       L/2       L/10        0        WR
GW108   10      -L/2       L/5        0       L/2       L/5         0        WR
GW109   10      -L/2       3L/10      0       L/2       3L/10       0        WR
GW110   10      -L/2       2L/5       0       L/2       2L/5        0        WR
GW111   10      -L/2       L/2        0       L/2       L/2         0        WR
GW112   10      -L/2      -L/2        0      -L/2       L/2         0        WR
GW113   10     -2L/5      -L/2        0     -2L/5       L/2         0        WR
GW114   10     -3L/10     -L/2        0     -3L/10      L/2         0        WR
```

```
GW115   10      -L/5    -L/2    0       -L/5    L/2     0       WR
GW116   10      -L/10   -L/2    0       -L/10   L/2     0       WR
GW117   10      0       -L/2    0       0       L/2     0       WR
GW118   10      L/10    -L/2    0       L/10    L/2     0       WR
GW119   10      L/5     -L/2    0       L/5     L/2     0       WR
GW120   10      3L/10   -L/2    0       3L/10   L/2     0       WR
GW121   10      2L/5    -L/2    0       2L/5    L/2     0       WR
GW122   10      L/2     -L/2    0       L/2     L/2     0       WR
GW130   1       D       0       H       D       0       0       R
GW930   1       D       0       0       L/10    L/10    0       WR
GW931   1       D       0       0       L/5     L/10    0       WR
GW932   1       D       0       0       L/10    -L/10   0       WR
GW933   1       D       0       0       L/5     -L/10   0       WR
GE  0
EX  0   130     1   0   1.      0.      0.      0.      0.      0.
FR  0   1       0   0   2400    50
RP  0   73      2 1001  0       0       5       90
EN
```

Appendix D

NEC Input File for 435 MHz Helix

```
CM 435MHz HELIX N=13 D=10.4CM S=15.2CM HEIGHT ON PLANE IS 5mm
CM FC is 435MHz WL=68.92cm wire radius is 3.175mm
CM USE 1 WAVELENGTH PLANE GRID BY 0.1WL SO WR=WL/22PI=0.997CM
CM LH=13S=1.976M
CM sweep freq. from 400MHz to 450MHz
CM  5    10   15   20        30        40        50        60        70        80
CM  v    v    v    v         v         v         v         v         v         v
CM---_____-----____----------_________----------_________----------_________
CE
SY  F=435
SY  LH=1.976
SY  L=0.6892
SY  D=0.104
SY  R=.003175
SY  WR=0.00997
SY  S=0.152
SY  H=0.005
GH 88  200       S        LH        D         D         D         D         R
GM 88    0       0         0        0         0         0         H
GW  1   10     -L/2      -L/2       0       L/2      -L/2         0        WR
GW  2   10     -L/2     -2L/5       0       L/2     -2L/5         0        WR
GW  3   10     -L/2    -3L/10       0       L/2    -3L/10         0        WR
GW  4   10     -L/2      -L/5       0       L/2      -L/5         0        WR
GW  5   10     -L/2     -L/10       0       L/2     -L/10         0        WR
GW  6   10     -L/2         0       0       L/2         0         0        WR
GW  7   10     -L/2       L/10      0       L/2       L/10        0        WR
GW  8   10     -L/2       L/5       0       L/2       L/5         0        WR
GW  9   10     -L/2      3L/10      0       L/2      3L/10        0        WR
GW 10   10     -L/2      2L/5       0       L/2      2L/5         0        WR
GW 11   10     -L/2       L/2       0       L/2       L/2         0        WR
GW 12   10     -L/2      -L/2       0      -L/2       L/2         0        WR
GW 13   10    -2L/5      -L/2       0     -2L/5       L/2         0        WR
GW 14   10    -3L/10     -L/2       0     -3L/10      L/2         0        WR
GW 15   10     -L/5      -L/2       0      -L/5       L/2         0        WR
GW 16   10     -L/10     -L/2       0      -L/10      L/2         0        WR
GW 17   10       0       -L/2       0        0        L/2         0        WR
GW 18   10      L/10     -L/2       0       L/10      L/2         0        WR
GW 19   10      L/5      -L/2       0       L/5       L/2         0        WR
GW 20   10     3L/10     -L/2       0      3L/10      L/2         0        WR
GW 21   10     2L/5      -L/2       0      2L/5       L/2         0        WR
GW 22   10      L/2      -L/2       0       L/2       L/2         0        WR
GW 30    1        D         0       0       L/10      L/10        0        WR
GW 31    1        D         0       0       L/5       L/10        0        WR
```

```
GW 32    1        D        0        0      L/10     -L/10      0       WR
GW 33    1        D        0        0       L/5     -L/10      0       WR
GW 40    1        D        0        0         D         0      H        R
GE  0
EX  0   40    1   0       1.       0.        0.        0.      0.       0.
FR  0    1    0   0      435        2
RP  0   73    2 1001        0        0         5        90
EN
```

Appendix E

Brief NEC2 Output File for 2.4 GHz Helix

------FREQUENCY------

FREQUENCY= 2.4000E+03 MHZ

WAVELENGTH= 1.2492E-01 METERS

APPROXIMATE INTEGRATION EMPLOYED FOR SEGMENTS MORE THAN 1.000 WAVELENGTHS APART

---STRUCTURE IMPEDANCE LOADING---

THIS STRUCTURE IS NOT LOADED

---ANTENNA ENVIRONMENT---

FREE SPACE

---MATRIX TIMING---

FILL= 0.541 SEC., FACTOR= 0.150 SEC.

---ANTENNA INPUT PARAMETERS---

TAG	SEG	VOLTAGE (VOLTS)		CURRENT (AMPS)		IMPEDANCE (OHMS)		ADMITTANCE (MHOS)		POWER
NO.	NO.	REAL	IMAG	REAL	IMAG	REAL	IMAG	REAL	IMAG	(WATTS)
130	311	1.00000E+00	0.00000E+00	6.03515E-03	2.72820E-03	1.37581E+02	-6.21939E+01	6.03515E-03	2.72820E-03	3.01758E-03

---POWER BUDGET---

INPUT POWER = 3.0176E-03 WATTS

RADIATED POWER= 3.0176E-03 WATTS

STRUCTURE LOSS= 0.0000E+00 WATTS

NETWORK LOSS = 0.0000E+00 WATTS

EFFICIENCY = 100.00 PERCENT

---RADIATION PATTERNS---

--ANGLES-- -POWER GAINS- ---POLARIZATION--- ---E(THETA)--- ---E(PHI)---

THETA	PHI	VERT.	HOR.	TOTAL	AXIAL	TILT	SENSE	MAGNITUDE	PHASE	MAGNITUDE	PHASE
DEGREES	DEGREES	DB	DB	DB	TIO	DEG		VOLTS/M	DEGREES	VOLTS/M	DEGREES
0.00	0.00	9.25	7.26	11.38	0.79534	0.56	RIGHT	1.23348E+00	-157.71	9.81081E-01	112.55
5.00	0.00	9.16	7.09	11.26	0.78734	1.01	RIGHT	1.22148E+00	-158.33	9.61863E-01	112.15
10.00	0.00	8.73	6.58	10.80	0.78037	2.65	RIGHT	1.16159E+00	-160.55	9.07465E-01	110.77
15.00	0.00	7.91	5.71	9.96	0.77254	5.71	RIGHT	1.05694E+00	-164.39	8.20896E-01	108.57
20.00	0.00	6.64	4.42	8.68	0.75933	10.60	RIGHT	9.13902E-01	-169.95	7.07617E-01	105.81
25.00	0.00	4.84	2.63	6.88	0.73028	17.65	RIGHT	7.42272E-01	-177.45	5.75943E-01	103.01
30.00	0.00	2.31	0.24	4.41	0.66376	26.44	RIGHT	5.55178E-01	172.61	4.37262E-01	101.18
35.00	0.00	-1.24	-2.86	1.04	0.52051	35.67	RIGHT	3.68646E-01	158.90	3.06158E-01	102.46
40.00	0.00	-6.46	-6.51	-3.47	0.22494	44.84	RIGHT	2.02129E-01	136.67	2.01118E-01	111.31
45.00	0.00	-13.21	-9.44	-7.91	0.40283	62.29	LEFT	9.29638E-02	82.68	1.43549E-01	132.11
50.00	0.00	-11.65	-10.02	-7.75	0.28450	-51.30	LEFT	1.11284E-01	6.32	1.34241E-01	153.93
55.00	0.00	-8.51	-9.78	-6.09	0.09772	-40.76	RIGHT	1.59657E-01	-26.54	1.38009E-01	164.74
60.00	0.00	-7.58	-10.12	-5.66	0.31496	-34.87	RIGHT	1.77722E-01	-46.76	1.32737E-01	169.94
65.00	0.00	-8.25	-10.86	-6.35	0.52443	-29.53	RIGHT	1.64603E-01	-62.76	1.21800E-01	176.58
70.00	0.00	-10.29	-10.98	-7.61	0.83597	-31.66	RIGHT	1.30089E-01	-74.91	1.20119E-01	-174.06
75.00	0.00	-13.71	-10.00	-8.46	0.65231	-89.92	RIGHT	8.77303E-02	-79.19	1.34491E-01	-169.26
80.00	0.00	-17.58	-8.79	-8.25	0.33533	-81.92	RIGHT	5.62162E-02	-63.52	1.54546E-01	-173.75
85.00	0.00	-17.28	-8.09	-7.60	0.14660	-72.50	RIGHT	5.81859E-02	-33.23	1.67502E-01	174.35
90.00	0.00	-14.47	-8.12	-7.21	0.00780	-64.30	RIGHT	8.03813E-02	-23.51	1.67029E-01	157.63
95.00	0.00	-12.35	-8.89	-7.28	0.13854	-56.58	LEFT	1.02580E-01	-25.35	1.52759E-01	137.57
100.00	0.00	-10.86	-10.42	-7.62	0.32081	-46.79	LEFT	1.21849E-01	-29.70	1.28184E-01	114.67
105.00	0.00	-9.61	-12.68	-7.87	0.49076	-28.11	LEFT	1.40746E-01	-34.21	9.87492E-02	88.53
110.00	0.00	-8.42	-15.62	-7.66	0.43252	-3.48	LEFT	1.61344E-01	-39.10	7.04465E-02	57.40
115.00	0.00	-7.35	-18.75	-7.05	0.23650	7.35	LEFT	1.82452E-01	-45.13	4.91219E-02	18.02
120.00	0.00	-6.57	-20.69	-6.40	0.07492	10.31	LEFT	1.99706E-01	-52.55	3.92835E-02	-29.38
125.00	0.00	-6.23	-20.67	-6.08	0.03716	10.54	RIGHT	2.07546E-01	-61.21	3.93658E-02	-72.90
130.00	0.00	-6.50	-19.95	-6.30	0.11568	10.10	RIGHT	2.01336E-01	-70.92	4.27678E-02	-105.09
135.00	0.00	-7.52	-19.37	-7.25	0.17927	10.35	RIGHT	1.78881E-01	-81.93	4.57440E-02	-128.29
140.00	0.00	-9.56	-19.00	-9.09	0.24379	13.18	RIGHT	1.41451E-01	-95.68	4.77467E-02	-145.09
145.00	0.00	-12.96	-18.70	-11.93	0.27750	23.73	RIGHT	9.56942E-02	-117.64	4.93783E-02	-156.86
150.00	0.00	-16.41	-18.36	-14.26	0.00567	38.63	LEFT	6.43305E-02	-165.27	5.14029E-02	-164.60
155.00	0.00	-13.72	-17.87	-12.31	0.39847	26.12	LEFT	8.76136E-02	140.34	5.43264E-02	-169.50
160.00	0.00	-9.71	-17.28	-9.01	0.38446	9.47	LEFT	1.39152E-01	116.98	5.82017E-02	-172.82
165.00	0.00	-7.03	-16.63	-6.58	0.32195	4.42	LEFT	1.89340E-01	106.54	6.26699E-02	-175.53
170.00	0.00	-5.40	-16.02	-5.04	0.28971	3.02	LEFT	2.28320E-01	101.27	6.72265E-02	-178.18
175.00	0.00	-4.56	-15.48	-4.22	0.27946	3.01	LEFT	2.51587E-01	98.98	7.15352E-02	179.16
180.00	0.00	-4.37	-15.01	-4.01	0.28615	3.88	LEFT	2.57090E-01	99.04	7.55920E-02	176.81
185.00	0.00	-4.80	-14.55	-4.37	0.31008	5.67	LEFT	2.44683E-01	101.48	7.96329E-02	175.48
190.00	0.00	-5.88	-14.11	-5.27	0.35515	8.96	LEFT	2.16108E-01	106.94	8.38418E-02	176.21

195.00	0.00	-7.69	-13.67	-6.71	0.42044	15.68	LEFT	1.75525E-01	117.14	8.81153E-02	-179.85
200.00	0.00	-10.19	-13.28	-8.46	0.44278	29.72	LEFT	1.31578E-01	136.29	9.21642E-02	-171.73
205.00	0.00	-12.30	-12.94	-9.60	0.26517	42.60	LEFT	1.03159E-01	171.33	9.59160E-02	-158.88
210.00	0.00	-11.46	-12.59	-8.98	0.04436	41.25	LEFT	1.13712E-01	-146.44	9.97845E-02	-141.31
215.00	0.00	-8.96	-12.21	-7.27	0.01952	34.51	RIGHT	1.51690E-01	-117.33	1.04309E-01	-119.73
220.00	0.00	-6.94	-11.81	-5.71	0.02281	29.70	LEFT	1.91410E-01	-98.21	1.09245E-01	-95.17
225.00	0.00	-5.74	-11.51	-4.72	0.10571	26.78	LEFT	2.19606E-01	-83.28	1.13085E-01	-68.40
230.00	0.00	-5.30	-11.44	-4.35	0.21323	24.08	LEFT	2.31173E-01	-70.23	1.13934E-01	-39.27
235.00	0.00	-5.48	-11.63	-4.54	0.34825	19.46	LEFT	2.26327E-01	-58.42	1.11446E-01	-6.82
240.00	0.00	-6.15	-11.86	-5.11	0.49872	8.25	LEFT	2.09615E-01	-48.03	1.08580E-01	29.90
245.00	0.00	-7.07	-11.69	-5.78	0.52717	-15.23	LEFT	1.88539E-01	-39.43	1.10723E-01	69.72
250.00	0.00	-7.92	-10.99	-6.18	0.33072	-32.52	LEFT	1.70812E-01	-32.33	1.20054E-01	108.34
255.00	0.00	-8.48	-10.22	-6.25	0.10912	-39.15	LEFT	1.60301E-01	-25.13	1.31165E-01	142.16
260.00	0.00	-8.80	-9.98	-6.34	0.05351	-41.08	RIGHT	1.54487E-01	-15.81	1.34780E-01	170.38
265.00	0.00	-9.25	-10.74	-6.92	0.14412	-39.91	RIGHT	1.46614E-01	-3.90	1.23528E-01	-167.25
270.00	0.00	-10.30	-12.93	-8.41	0.14440	-36.08	RIGHT	1.29922E-01	8.94	9.59829E-02	-153.84
275.00	0.00	-12.50	-16.30	-10.98	0.01472	-32.84	LEFT	1.00891E-01	18.60	6.51422E-02	-163.25
280.00	0.00	-16.26	-14.86	-12.49	0.25795	-50.26	LEFT	6.54371E-02	12.29	7.68757E-02	162.95
285.00	0.00	-16.48	-10.27	-9.33	0.03704	-63.99	RIGHT	6.38189E-02	-28.02	1.30441E-01	157.35
290.00	0.00	-11.30	-7.21	-5.78	0.22096	-59.45	RIGHT	1.15870E-01	-41.22	1.85438E-01	166.74
295.00	0.00	-7.62	-5.64	-3.51	0.28013	-52.58	RIGHT	1.76919E-01	-32.35	2.22080E-01	179.86
300.00	0.00	-5.56	-5.40	-2.46	0.26873	-45.61	RIGHT	2.24384E-01	-16.70	2.28556E-01	-166.61
305.00	0.00	-4.74	-6.63	-2.57	0.19640	-38.28	RIGHT	2.46567E-01	2.91	1.98181E-01	-154.30
310.00	0.00	-4.90	-10.31	-3.80	0.04561	-28.14	RIGHT	2.41951E-01	27.77	1.29839E-01	-145.96
315.00	0.00	-5.38	-21.37	-5.28	0.13126	-5.10	LEFT	2.28845E-01	61.65	3.63130E-02	-174.83
320.00	0.00	-4.47	-11.32	-3.65	0.12288	23.67	RIGHT	2.54301E-01	103.36	1.15604E-01	84.62
325.00	0.00	-1.65	-4.12	0.30	0.46224	32.31	RIGHT	3.51868E-01	138.38	2.64576E-01	85.92
330.00	0.00	1.43	-0.08	3.75	0.66506	31.75	RIGHT	5.01751E-01	161.33	4.21508E-01	91.90
335.00	0.00	3.99	2.60	6.36	0.77239	25.62	RIGHT	6.73167E-01	176.37	5.73889E-01	97.88
340.00	0.00	5.94	4.47	8.28	0.81595	16.50	RIGHT	8.43220E-01	-173.33	7.11486E-01	103.03
345.00	0.00	7.38	5.77	9.66	0.82281	8.62	RIGHT	9.95032E-01	-166.21	8.26108E-01	107.13
350.00	0.00	8.38	6.62	10.60	0.81539	3.78	RIGHT	1.11607E+00	-161.47	9.11683E-01	110.08
355.00	0.00	8.99	7.11	11.16	0.80495	1.35	RIGHT	1.19743E+00	-158.71	9.64119E-01	111.88
360.00	0.00	9.25	7.26	11.38	0.79534	0.56	RIGHT	1.23348E+00	-157.71	9.81081E-01	112.55

Appendix F

Brief NEC2 Output File for 435 MHz Helix

------ FREQUENCY ------

FREQUENCY= 4.3500E+02 MHZ
WAVELENGTH= 6.8920E-01 METERS

APPROXIMATE INTEGRATION EMPLOYED FOR SEGMENTS MORE THAN 1.000 WAVELENGTHS APART

--- STRUCTURE IMPEDANCE LOADING ---
THIS STRUCTURE IS NOT LOADED

--- ANTENNA ENVIRONMENT ---

FREE SPACE

--- MATRIX TIMING ---

FILL= 0.771 SEC., FACTOR= 0.441 SEC.

--- ANTENNA INPUT PARAMETERS ---

TAG NO.	SEG NO.	VOLTAGE (VOLTS) REAL	VOLTAGE (VOLTS) IMAG.	CURRENT (AMPS) REAL	CURRENT (AMPS) IMAG.	IMPEDANCE (OHMS) REAL	IMPEDANCE (OHMS) IMAG.	ADMITTANCE (MHOS) REAL	ADMITTANCE (MHOS) IMAG.	POWER (WATTS)
40	425	1.00000E+00	0.00000E+00	6.39912E-03	5.46312E-03	9.03901E+01	-7.71689E+01	6.39912E-03	5.46312E-03	3.19956E

--- POWER BUDGET ---

INPUT POWER = 3.1996E-03 WATTS
RADIATED POWER= 3.1996E-03 WATTS
STRUCTURE LOSS= 0.0000E+00 WATTS
NETWORK LOSS = 0.0000E+00 WATTS
EFFICIENCY = 100.00 PERCENT

--- RADIATION PATTERNS ---

- - ANGLES - - -		POWER GAINS - - - -			POLARIZATION - - - - - -			E(THETA) - - -		- - - E(PHI) - - -	
THETA	PHI	VERT.	HOR.	TOTAL	AXIAL	TILT	SENSE	MAGNITUDE	PHASE	MAGNITUDE	PHASE
DEGREES	DEGREES	DB	DB	DB	RATIO	DEG		VOLTS/M	DEGREES	VOLTS/M	DEGREES
0.00	0.00	9.27	9.44	12.37	0.95082	56.54	RIGHT	1.27386E+00	94.56	1.29929E+00	7.22
5.00	0.00	9.12	9.35	12.25	0.93872	57.04	RIGHT	1.25222E+00	92.81	1.28491E+00	6.11
10.00	0.00	8.55	8.96	11.77	0.92116	62.48	RIGHT	1.17207E+00	89.35	1.22845E+00	3.21
15.00	0.00	7.48	8.18	10.86	0.89662	69.17	RIGHT	1.03601E+00	84.41	1.12385E+00	-1.43
20.00	0.00	5.77	6.86	9.36	0.86757	75.84	RIGHT	8.51489E-01	78.57	9.64738E-01	-7.56
25.00	0.00	3.25	4.68	7.03	0.84401	83.21	RIGHT	6.36561E-01	73.38	7.50575E-01	-14.33
30.00	0.00	-0.23	1.09	3.49	0.85756	-85.18	RIGHT	4.26656E-01	72.70	4.96428E-01	-18.78
35.00	0.00	-3.89	-4.62	-1.23	0.91759	-5.42	RIGHT	2.79957E-01	83.75	2.57281E-01	-7.18
40.00	0.00	-5.28	-5.98	-2.61	0.54565	40.73	RIGHT	2.38379E-01	100.85	2.19922E-01	43.32
45.00	0.00	-5.54	-1.99	-0.40	0.40327	61.24	RIGHT	2.31578E-01	103.33	3.48239E-01	54.55
50.00	0.00	-7.37	-0.67	0.17	0.33474	72.10	RIGHT	1.87559E-01	95.58	4.05541E-01	43.39
55.00	0.00	-11.62	-2.01	-1.55	0.29077	81.03	RIGHT	1.14928E-01	92.72	3.47710E-01	28.59
60.00	0.00	-15.40	-6.11	-5.63	0.34293	-89.27	RIGHT	7.43845E-02	115.61	2.16761E-01	23.73
65.00	0.00	-14.86	-8.89	-7.91	0.46166	78.44	RIGHT	7.91109E-02	125.83	1.57371E-01	54.33
70.00	0.00	-17.15	-5.73	-5.43	0.20129	79.90	RIGHT	6.08147E-02	113.96	2.26403E-01	63.41
75.00	0.00	-26.12	-4.89	-4.86	0.08616	89.38	RIGHT	2.16575E-02	129.54	2.49401E-01	46.65
80.00	0.00	-21.62	-7.09	-6.94	0.03356	-79.53	RIGHT	3.63513E-02	-161.39	1.93540E-01	29.26
85.00	0.00	-18.45	-10.85	-10.15	0.09273	-67.86	RIGHT	5.23768E-02	-162.12	1.25603E-01	32.88
90.00	0.00	-16.88	-9.91	-9.11	0.11070	-66.50	RIGHT	6.27347E-02	-151.13	1.40010E-01	45.91
95.00	0.00	-13.33	-8.22	-7.05	0.02586	-60.98	LEFT	9.43898E-02	-147.10	1.69964E-01	29.41
100.00	0.00	-10.88	-8.87	-6.75	0.19609	-52.11	LEFT	1.25150E-01	-154.28	1.57735E-01	2.90
105.00	0.00	-9.45	-11.37	-7.29	0.35862	-36.79	LEFT	1.47640E-01	-158.17	1.18271E-01	-18.80
110.00	0.00	-7.49	-13.39	-6.49	0.31435	-21.94	LEFT	1.85001E-01	-159.96	9.37732E-02	-25.15
115.00	0.00	-5.46	-12.26	-4.63	0.29446	-19.41	LEFT	2.33671E-01	-167.92	1.06735E-01	-33.72
120.00	0.00	-4.43	-10.77	-3.52	0.38077	-16.73	LEFT	2.63013E-01	-179.63	1.26756E-01	-57.87
125.00	0.00	-4.46	-10.46	-3.49	0.48438	-7.53	LEFT	2.62141E-01	170.44	1.31352E-01	-87.96
130.00	0.00	-4.98	-11.41	-4.09	0.45931	7.53	LEFT	2.46836E-01	164.63	1.17763E-01	-117.96
135.00	0.00	-5.52	-13.42	-4.87	0.30761	14.65	LEFT	2.32065E-01	160.17	9.33745E-02	-145.59
140.00	0.00	-6.34	-16.01	-5.90	0.18442	15.25	LEFT	2.10988E-01	152.55	6.93697E-02	-170.50
145.00	0.00	-8.13	-18.00	-7.71	0.13281	16.31	LEFT	1.71714E-01	139.46	5.51288E-02	166.11
150.00	0.00	-11.36	-18.03	-10.51	0.17911	23.24	LEFT	1.18493E-01	116.64	5.49785E-02	143.68
155.00	0.00	-14.54	-16.21	-12.29	0.50197	35.77	LEFT	8.20904E-02	70.12	6.77830E-02	124.87
160.00	0.00	-12.38	-13.88	-10.06	0.83938	-4.18	LEFT	1.05327E-01	19.65	8.85775E-02	111.12
165.00	0.00	-8.96	-11.89	-7.18	0.65596	-17.65	LEFT	1.56070E-01	-2.32	1.11382E-01	101.77
170.00	0.00	-6.70	-10.47	-5.18	0.58612	-16.58	LEFT	2.02532E-01	-10.97	1.31162E-01	96.06
175.00	0.00	-5.36	-9.63	-3.98	0.55631	-15.18	LEFT	2.36303E-01	-13.83	1.44616E-01	93.58
180.00	0.00	-4.70	-9.29	-3.40	0.53810	-14.20	LEFT	2.55082E-01	-13.25	1.50289E-01	94.18
185.00	0.00	-4.58	-9.40	-3.34	0.52446	-13.80	LEFT	2.58412E-01	-9.90	1.48432E-01	97.86

190.00	0.00	-4.97	-9.86	-3.75	0.51809	-13.96	LEFT	2.47027E-01	-3.62	1.40782E-01	104.67
195.00	0.00	-5.85	-10.54	-4.58	0.52989	-14.37	LEFT	2.23246E-01	6.41	1.30209E-01	114.48
200.00	0.00	-7.16	-11.24	-5.73	0.58069	-13.94	LEFT	1.92066E-01	21.69	1.20051E-01	126.63
205.00	0.00	-8.61	-11.75	-6.89	0.68630	-7.51	LEFT	1.62613E-01	43.98	1.13178E-01	139.68
210.00	0.00	-9.50	-11.89	-7.52	0.71760	16.43	LEFT	1.46730E-01	72.54	1.11371E-01	152.15
215.00	0.00	-9.35	-11.61	-7.32	0.57451	29.81	LEFT	1.49305E-01	100.74	1.15072E-01	164.03
220.00	0.00	-8.56	-11.10	-6.64	0.48652	31.33	LEFT	1.63426E-01	122.22	1.22097E-01	177.36
225.00	0.00	-7.57	-10.81	-5.88	0.48588	27.39	LEFT	1.83247E-01	137.24	1.26223E-01	-165.46
230.00	0.00	-6.51	-11.27	-5.26	0.49835	16.99	LEFT	2.06989E-01	150.04	1.19622E-01	-142.82
235.00	0.00	-5.76	-12.88	-4.99	0.43506	3.99	LEFT	2.25729E-01	164.31	9.94148E-02	-113.06
240.00	0.00	-5.80	-15.45	-5.35	0.31225	-5.96	LEFT	2.24639E-01	179.89	7.39219E-02	-73.49
245.00	0.00	-6.78	-17.31	-6.41	0.18420	-13.16	LEFT	2.00677E-01	-167.04	5.96676E-02	-27.74
250.00	0.00	-7.97	-16.91	-7.45	0.09829	-18.97	LEFT	1.74973E-01	-160.72	6.25308E-02	1.39
255.00	0.00	-8.27	-13.96	-7.23	0.08428	-27.16	LEFT	1.69081E-01	-156.35	8.78233E-02	11.85
260.00	0.00	-8.56	-10.21	-6.30	0.06012	-39.55	LEFT	1.63401E-01	-146.40	1.35134E-01	26.60
265.00	0.00	-10.15	-8.08	-5.98	0.04125	-51.78	RIGHT	1.36171E-01	-138.47	1.72766E-01	46.39
270.00	0.00	-11.48	-8.11	-6.46	0.22343	-57.04	RIGHT	1.16870E-01	-145.77	1.72213E-01	61.49
275.00	0.00	-10.22	-8.92	-6.51	0.25396	-49.88	RIGHT	1.35050E-01	-150.16	1.56909E-01	58.69
280.00	0.00	-10.03	-6.80	-5.11	0.09696	-55.62	RIGHT	1.38059E-01	-142.00	2.00228E-01	49.87
285.00	0.00	-12.24	-4.40	-3.74	0.14610	-69.26	RIGHT	1.06983E-01	-145.42	2.63960E-01	58.84
290.00	0.00	-11.46	-4.36	-3.58	0.38274	-77.42	RIGHT	1.17076E-01	-171.63	2.65231E-01	73.01
295.00	0.00	-8.49	-6.76	-4.53	0.63117	-58.63	RIGHT	1.64718E-01	-173.94	2.01112E-01	73.10
300.00	0.00	-8.37	-6.47	-4.30	0.29555	-52.44	RIGHT	1.67137E-01	-168.77	2.08053E-01	45.06
305.00	0.00	-9.91	-2.52	-1.79	0.26495	-71.36	RIGHT	1.39994E-01	176.97	3.27692E-01	40.22
310.00	0.00	-7.71	-0.70	0.09	0.43657	-84.66	RIGHT	1.80235E-01	151.93	4.04042E-01	52.19
315.00	0.00	-5.00	-1.54	0.08	0.66052	82.45	RIGHT	2.46270E-01	148.16	3.66955E-01	64.50
320.00	0.00	-4.68	-5.54	-2.08	0.87937	19.50	RIGHT	2.55681E-01	147.13	2.31421E-01	61.77
325.00	0.00	-5.57	-6.90	-3.18	0.52865	-37.16	RIGHT	2.30641E-01	128.46	1.97827E-01	5.19
330.00	0.00	-2.89	-0.22	1.66	0.59178	-64.08	RIGHT	3.14145E-01	97.27	4.26848E-01	-16.08
335.00	0.00	1.55	3.94	5.92	0.72471	-74.78	RIGHT	5.23779E-01	86.61	6.89673E-01	-12.81
340.00	0.00	4.81	6.41	8.70	0.82415	-81.08	RIGHT	7.62380E-01	87.09	9.16291E-01	-6.32
345.00	0.00	6.95	7.91	10.46	0.89500	-87.37	RIGHT	9.74677E-01	90.17	1.08851E+00	-0.42
350.00	0.00	8.27	8.79	11.55	0.93964	82.35	RIGHT	1.13535E+00	93.00	1.20561E+00	3.94
355.00	0.00	9.01	9.27	12.15	0.95573	66.24	RIGHT	1.23541E+00	94.59	1.27376E+00	6.50
360.00	0.00	9.27	9.44	12.37	0.95082	56.54	RIGHT	1.27386E+00	94.56	1.29929E+00	7.22

Appendix G

Input File for REF.FOR, to Calculate the Reflector Radiation Pattern

```
CM: *** O60C.DAT ***
CE: OFFSET CIRCULAR 30" REFLECTOR AT C-BAND
RG:
1    0.76    0.446
1    0.01    0.01
TL: TILT ANGLE AND OFFSET
66.3        0.392                          ;PSIT,YC
FG:
1    2.4
FP:
T          T          T          1      90.        ;LCP=T
2   0.   90.
73
     0.00      11.38       0.56          0.00      11.38     -89.44
     5.00      11.26       1.01          5.00      11.15     -87.81
    10.00      10.80       2.65         10.00      10.58     -86.20
    15.00       9.96       5.71         15.00       9.64     -84.68
    20.00       8.68      10.60         20.00       8.25     -83.13
    25.00       6.88      17.65         25.00       6.28     -81.36
    30.00       4.41      26.44         30.00       3.49     -79.10
    35.00       1.04      35.67         35.00      -0.59     -75.92
    40.00      -3.47      44.84         40.00      -7.05     -72.48
    45.00      -7.91      62.29         45.00     -11.12      57.17
    50.00      -7.75     -51.30         50.00      -5.50      70.63
    55.00      -6.09     -40.76         55.00      -2.42      83.64
    60.00      -5.66     -34.87         60.00      -1.06     -88.80
    65.00      -6.35     -29.53         65.00      -0.73     -82.79
    70.00      -7.61     -31.66         70.00      -1.12     -76.42
    75.00      -8.46     -89.92         75.00      -2.10     -68.19
    80.00      -8.25     -81.92         80.00      -3.59     -56.15
    85.00      -7.60     -72.50         85.00      -5.54     -39.50
    90.00      -7.21     -64.30         90.00      -7.70     -23.90
    95.00      -7.28     -56.58         95.00      -9.37     -17.19
   100.00      -7.62     -46.79        100.00      -9.66     -22.63
   105.00      -7.87     -28.11        105.00      -8.91     -29.29
   110.00      -7.66      -3.48        110.00      -8.12     -28.26
   115.00      -7.05       7.35        115.00      -7.73     -23.26
   120.00      -6.40      10.31        120.00      -7.85     -16.38
   125.00      -6.08      10.54        125.00      -8.47      -7.70
   130.00      -6.30      10.10        130.00      -9.49       4.18
   135.00      -7.25      10.35        135.00     -10.66      21.76
   140.00      -9.09      13.18        140.00     -11.37      44.61
   145.00     -11.93      23.73        145.00     -10.99      65.53
   150.00     -14.26      38.63        150.00      -9.68      79.43
```

155.00	-12.31	26.12	155.00	-8.11	86.60
160.00	-9.01	9.47	160.00	-6.68	89.51
165.00	-6.58	4.42	165.00	-5.54	-89.53
170.00	-5.04	3.02	170.00	-4.72	-88.96
175.00	-4.22	3.01	175.00	-4.21	-87.93
180.00	-4.01	3.88	180.00	-4.01	-86.12
185.00	-4.37	5.67	185.00	-4.11	-83.56
190.00	-5.27	8.96	190.00	-4.48	-80.63
195.00	-6.71	15.68	195.00	-5.13	-78.03
200.00	-8.46	29.72	200.00	-6.10	-76.79
205.00	-9.60	42.60	205.00	-7.42	-78.62
210.00	-8.98	41.25	210.00	-9.10	-86.60
215.00	-7.27	34.51	215.00	-10.83	75.69
220.00	-5.71	29.70	220.00	-11.49	51.59
225.00	-4.72	26.78	225.00	-10.34	23.46
230.00	-4.35	24.08	230.00	-8.58	1.47
235.00	-4.54	19.46	235.00	-7.24	-9.75
240.00	-5.11	8.25	240.00	-6.62	-16.35
245.00	-5.78	-15.23	245.00	-6.77	-21.27
250.00	-6.18	-32.52	250.00	-7.77	-25.10
255.00	-6.25	-39.15	255.00	-9.83	-26.16
260.00	-6.34	-41.08	260.00	-13.16	-19.14
265.00	-6.92	-39.91	265.00	-15.22	-21.17
270.00	-8.41	-36.08	270.00	-11.07	-63.55
275.00	-10.98	-32.84	275.00	-6.76	-76.37
280.00	-12.49	-50.26	280.00	-3.75	-83.35
285.00	-9.33	-63.99	285.00	-1.77	-88.92
290.00	-5.78	-59.45	290.00	-0.63	86.31
295.00	-3.51	-52.58	295.00	-0.31	82.07
300.00	-2.46	-45.61	300.00	-0.92	78.07
305.00	-2.57	-38.28	305.00	-2.77	73.60
310.00	-3.80	-28.14	310.00	-6.45	64.92
315.00	-5.28	-5.10	315.00	-8.98	-18.16
320.00	-3.65	23.67	320.00	-3.21	-37.98
325.00	0.30	32.31	325.00	1.65	-68.43
330.00	3.75	31.75	330.00	4.95	-84.12
335.00	6.36	25.62	335.00	7.28	-89.68
340.00	8.28	16.50	340.00	8.94	88.14
345.00	9.66	8.62	345.00	10.11	87.56
350.00	10.60	3.78	350.00	10.87	87.97
355.00	11.16	1.35	355.00	11.29	89.06
360.00	11.38	0.56	360.00	11.38	-89.44

CO: LAI=T, LGTD=F
T T F 0.
F F
0. 0.
OP:
1
0.
-180 180 1
0 F F
PD: PLOT DATA GENERATED
T ;LPLOT
XQ:

Appendix H

Brief Output Result for the Reflector Antenna Code

```
          *****  OUTPUT LISTING FROM REF.FOR VERSION 1.0  *****

*************************************************************************
 *  CO: LAI=T, LGTD=F                                                    *
*       LAI = T              LFEED = T        LGTD = F                  *
*       THETAX = 0.00                                                   *
*       LCORNR= F            LSLOPE= F                                    *
*       THEXF=     0.00    THEXR=     0.00                              *
*************************************************************************
 *************************************************************************
 *  OP:                                                                  *
  *   USING THE PRESENT GEOMETRY,THERE WILL BE     1 PATTERN CUTS COMPUTED
 *   THE FOLLOWING CUTS WILL BE COMPUTED:                                    *
 *       0.0,
 *       AP3I =-180.00      AP3F = 180.00                                *
 *   FOR EACH CUT THE PATTERN WILL BE COMPUTED EACH     1.00 DEGREES IN THETA
*
*       NTEST=   0           LSTEP2= F                                   *
*************************************************************************
 *************************************************************************
 *  PD: PLOT DATA GENERATED                                                *
*       DATA WILL BE OUTPUT TO OUT3.DAT FOR PLOTTING                        *
*************************************************************************
 *************************************************************************
 *  XQ:                                                                  *
 *          FREQUENCY =        2.400 GHZ                                   *
 *          WAVELENGTH =       0.125000 METERS                             *
 * THE FOLLOWING DIMENSION UNITS ARE IN WAVELENGTHS *                      *
 *       * ANGLES & PHASE ARE IN DEGREES *                                   *
 *          APERTURE RADII : RRW=          3.0400                         *
 *          FOCAL DISTANCE =       3.57                                    *
 *          GRIDX =    0.08       GRIDY =    0.08                          *
 *          DISTANCE FROM VERTEX TO APERTURE PLANE: ZOP=      2.673            *
 *          DISTANCE FROM FOCUS TO RIM: RO=      6.241                        *
 *       CIRCULARLY POLARIZED FEED                                           *
 *          FEED POWER: PRAD = 0.630E+01                                    *
 *          FAR FIELD GAIN REF =      -8.049                                *
 *          NUMBER OF PRINCIPAL GRID LINES: MMAX= 77        NMAX= 78            *
 *          APERTURE CENTER AT (     0.000,     3.136,     2.673,)          *
 *          SHADOW BOUNDARY ANGLES: TH1 =   180.00       TH2 =   180.00          *
 *          THEB (DEG) =    90.000                                          *
 *          NUMBER OF ROTATED GRID LINES: IMAX= 75        JMAX= 76              *
 *                                                                          *
```

```
*       AI/GTD SWITCHOVER PARAMETERS:                                   *
*         THETAX =    0.00                                               *
*           NT    = 361       P3X =      0.000                          *
*           NGTD1=    0       PG1I=      0.000                            *
*           NAI   = 361       PAI = -180.000                           *
*           NGTD2=    0       PG2I=      0.000                            *
*  PHI =      0.00                                                       *
W                                PRINCIPAL POL                CROSS POL                W
W                                                                                      W
W    THETA            MAG          DB          PHASE          MAG          DB          PHASE
W
*                                                                                      *
W   -180.00        0.241E-05   -120.51    -114.8   0.324E+01     2.05       46.5    W
W   -178.00        0.564E+00    -13.14    -114.0   0.319E+01     1.91       46.7    W
W   -176.00        0.105E+01     -7.76    -116.1   0.314E+01     1.76       47.2    W
W   -174.00        0.134E+01     -5.59    -121.1   0.308E+01     1.61       48.2    W
W   -172.00        0.142E+01     -5.13    -130.3   0.303E+01     1.46       49.6    W
W   -170.00        0.134E+01     -5.64    -145.7   0.298E+01     1.31       51.5    W
W   -168.00        0.125E+01     -6.21    -168.4   0.292E+01     1.15       53.7    W
W   -166.00        0.129E+01     -5.95     167.0   0.287E+01     0.98       56.3    W
W   -164.00        0.140E+01     -5.22     147.8   0.281E+01     0.81       59.3    W
W   -162.00        0.146E+01     -4.89     134.8   0.276E+01     0.64       62.7    W
W   -160.00        0.138E+01     -5.36     125.9   0.270E+01     0.46       66.4    W
W   -158.00        0.118E+01     -6.71     119.3   0.264E+01     0.28       70.5    W
W   -156.00        0.919E+00     -8.90     114.1   0.259E+01     0.09       75.0    W
W   -154.00        0.665E+00    -11.72     110.7   0.253E+01    -0.10       79.8    W
W   -152.00        0.480E+00    -14.54     110.8   0.247E+01    -0.30       84.9    W
W   -150.00        0.399E+00    -16.14     116.2   0.241E+01    -0.51       90.3    W
W   -148.00        0.425E+00    -15.59     123.1   0.236E+01    -0.72       95.8    W
W   -146.00        0.523E+00    -13.80     126.3   0.229E+01    -0.96       99.8    W
W   -144.00        0.642E+00    -12.01     126.2   0.223E+01    -1.20      103.8    W
W   -142.00        0.743E+00    -10.75     124.7   0.217E+01    -1.44      107.7    W
W   -140.00        0.797E+00    -10.14     122.7   0.211E+01    -1.68      111.5    W
W   -138.00        0.795E+00    -10.16     120.5   0.205E+01    -1.93      115.1    W
W   -136.00        0.744E+00    -10.73     118.2   0.199E+01    -2.18      118.6    W
W   -134.00        0.661E+00    -11.76     115.9   0.194E+01    -2.43      121.9    W
W   -132.00        0.565E+00    -13.12     113.7   0.188E+01    -2.68      125.0    W
W   -130.00        0.477E+00    -14.60     111.9   0.183E+01    -2.93      128.1    W
W   -128.00        0.409E+00    -15.93     111.0   0.179E+01    -3.13      136.2    W
W   -126.00        0.370E+00    -16.81     111.5   0.175E+01    -3.31      144.5    W
W   -124.00        0.360E+00    -17.04     113.3   0.171E+01    -3.49      153.0    W
W   -122.00        0.377E+00    -16.64     115.6   0.168E+01    -3.66      161.7    W
W   -120.00        0.414E+00    -15.83     117.6   0.165E+01    -3.82      170.6    W
W   -118.00        0.463E+00    -14.85     119.0   0.162E+01    -3.97      179.7    W
W   -116.00        0.516E+00    -13.91     119.8   0.159E+01    -4.11     -171.0    W
W   -114.00        0.568E+00    -13.07     120.1   0.158E+01    -4.22     -161.3    W
W   -112.00        0.615E+00    -12.39     120.1   0.156E+01    -4.30     -151.5    W
W   -110.00        0.653E+00    -11.86     119.9   0.155E+01    -4.37     -141.5    W
W   -108.00        0.684E+00    -11.47     119.5   0.154E+01    -4.41     -131.4    W
W   -106.00        0.706E+00    -11.18     119.1   0.153E+01    -4.44     -121.3    W
W   -104.00        0.723E+00    -10.98     118.7   0.153E+01    -4.46     -111.1    W
W   -102.00        0.735E+00    -10.85     118.3   0.153E+01    -4.46     -100.9    W
W   -100.00        0.743E+00    -10.75     117.9   0.153E+01    -4.48      -90.8    W
W    -98.00        0.750E+00    -10.66     117.6   0.153E+01    -4.49      -80.7    W
```

W	-96.00	0.757E+00	-10.58	117.3	0.153E+01	-4.47	-70.6	W
W	-94.00	0.765E+00	-10.49	117.1	0.154E+01	-4.44	-60.6	W
W	-92.00	0.775E+00	-10.38	117.0	0.154E+01	-4.39	-50.5	W
W	-90.00	0.788E+00	-10.24	117.0	0.156E+01	-4.33	-40.6	W
W	-88.00	0.803E+00	-10.08	117.0	0.155E+01	-4.36	-29.1	W
W	-86.00	0.821E+00	-9.88	117.1	0.154E+01	-4.39	-17.7	W
W	-84.00	0.841E+00	-9.67	117.3	0.154E+01	-4.44	-6.3	W
W	-82.00	0.863E+00	-9.45	117.6	0.153E+01	-4.50	4.9	W
W	-80.00	0.886E+00	-9.22	117.9	0.151E+01	-4.56	16.1	W
W	-78.00	0.907E+00	-9.01	118.3	0.150E+01	-4.64	27.2	W
W	-76.00	0.925E+00	-8.84	118.7	0.148E+01	-4.73	38.1	W
W	-74.00	0.938E+00	-8.73	119.1	0.147E+01	-4.83	48.9	W
W	-72.00	0.941E+00	-8.69	119.5	0.145E+01	-4.92	59.4	W
W	-70.00	0.933E+00	-8.77	119.9	0.144E+01	-5.01	69.6	W
W	-68.00	0.911E+00	-8.97	120.1	0.142E+01	-5.11	79.6	W
W	-66.00	0.875E+00	-9.32	120.1	0.141E+01	-5.20	89.2	W
W	-64.00	0.827E+00	-9.82	119.8	0.139E+01	-5.28	98.8	W
W	-62.00	0.771E+00	-10.43	119.0	0.139E+01	-5.32	108.7	W
W	-60.00	0.717E+00	-11.06	117.6	0.138E+01	-5.35	118.3	W
W	-58.00	0.680E+00	-11.52	115.6	0.138E+01	-5.37	127.4	W
W	-56.00	0.677E+00	-11.55	113.3	0.138E+01	-5.40	136.1	W
W	-54.00	0.725E+00	-10.95	111.5	0.137E+01	-5.41	144.4	W
W	-52.00	0.839E+00	-9.69	111.0	0.137E+01	-5.42	152.2	W
W	-50.00	0.102E+01	-7.97	111.9	0.137E+01	-5.42	159.6	W
W	-48.00	0.127E+01	-6.09	113.7	0.138E+01	-5.39	167.4	W
W	-46.00	0.156E+01	-4.32	115.9	0.138E+01	-5.35	174.7	W
W	-44.00	0.184E+01	-2.86	118.2	0.139E+01	-5.31	-178.5	W
W	-42.00	0.207E+01	-1.84	120.5	0.140E+01	-5.27	-172.2	W
W	-40.00	0.219E+01	-1.36	122.7	0.140E+01	-5.23	-166.4	W
W	-38.00	0.216E+01	-1.49	124.7	0.141E+01	-5.19	-161.1	W
W	-36.00	0.198E+01	-2.25	126.2	0.141E+01	-5.15	-156.3	W
W	-34.00	0.171E+01	-3.51	126.3	0.142E+01	-5.11	-152.0	W
W	-32.00	0.148E+01	-4.74	123.1	0.143E+01	-5.08	-148.2	W
W	-30.00	0.149E+01	-4.70	116.2	0.143E+01	-5.04	-145.1	W
W	-28.00	0.192E+01	-2.48	110.8	0.144E+01	-5.02	-142.5	W
W	-26.00	0.288E+01	1.02	110.7	0.144E+01	-4.99	-140.3	W
W	-24.00	0.432E+01	4.55	114.1	0.144E+01	-4.97	-138.5	W
W	-22.00	0.608E+01	7.51	119.3	0.145E+01	-4.95	-137.2	W
W	-20.00	0.784E+01	9.72	125.9	0.145E+01	-4.94	-136.3	W
W	-18.00	0.921E+01	11.12	134.8	0.145E+01	-4.92	-135.9	W
W	-16.00	0.999E+01	11.83	147.8	0.145E+01	-4.91	-135.9	W
W	-14.00	0.105E+02	12.27	167.0	0.146E+01	-4.91	-136.4	W
W	-12.00	0.119E+02	13.36	-168.4	0.146E+01	-4.91	-137.3	W
W	-10.00	0.153E+02	15.52	-145.7	0.146E+01	-4.91	-138.7	W
W	-8.00	0.203E+02	17.98	-130.3	0.145E+01	-4.91	-140.6	W
W	-6.00	0.257E+02	20.02	-121.1	0.145E+01	-4.92	-142.8	W
W	-4.00	0.300E+02	21.38	-116.1	0.145E+01	-4.93	-145.5	W
W	-2.00	0.323E+02	22.02	-114.0	0.145E+01	-4.94	-148.7	W
W	0.00	0.320E+02	21.94	-114.3	0.145E+01	-4.96	-152.2	W
W	2.00	0.291E+02	21.12	-117.1	0.145E+01	-4.94	-154.8	W
W	4.00	0.244E+02	19.59	-123.0	0.145E+01	-4.93	-157.8	W
W	6.00	0.190E+02	17.40	-133.6	0.145E+01	-4.92	-161.2	W
W	8.00	0.143E+02	14.93	-151.0	0.145E+01	-4.91	-165.0	W
W	10.00	0.114E+02	13.00	-175.1	0.145E+01	-4.91	-169.2	W

W	12.00	0.104E+02	12.16	161.2	0.146E+01	-4.91	-173.9	W
W	14.00	0.984E+01	11.69	143.7	0.145E+01	-4.91	-179.0	W
W	16.00	0.886E+01	10.78	131.9	0.145E+01	-4.92	175.5	W
W	18.00	0.731E+01	9.11	123.7	0.145E+01	-4.92	169.5	W
W	20.00	0.548E+01	6.61	117.4	0.145E+01	-4.93	163.2	W
W	22.00	0.377E+01	3.37	112.6	0.145E+01	-4.95	156.5	W
W	24.00	0.247E+01	-0.30	110.1	0.145E+01	-4.96	149.3	W
W	26.00	0.171E+01	-3.50	112.3	0.144E+01	-4.98	141.8	W
W	28.00	0.147E+01	-4.84	119.4	0.144E+01	-5.01	133.9	W
W	30.00	0.159E+01	-4.12	125.1	0.143E+01	-5.04	125.7	W
W	32.00	0.187E+01	-2.73	126.5	0.143E+01	-5.07	117.0	W
W	34.00	0.211E+01	-1.67	125.6	0.142E+01	-5.11	107.7	W
W	36.00	0.222E+01	-1.25	123.7	0.141E+01	-5.15	97.9	W
W	38.00	0.216E+01	-1.49	121.6	0.141E+01	-5.20	87.7	W
W	40.00	0.195E+01	-2.36	119.2	0.140E+01	-5.24	77.1	W
W	42.00	0.166E+01	-3.77	116.8	0.139E+01	-5.28	66.0	W
W	44.00	0.135E+01	-5.56	114.4	0.139E+01	-5.32	54.5	W
W	46.00	0.107E+01	-7.55	112.4	0.138E+01	-5.35	42.5	W
W	48.00	0.868E+00	-9.40	111.3	0.138E+01	-5.39	30.2	W
W	50.00	0.742E+00	-10.75	111.7	0.137E+01	-5.42	17.5	W
W	52.00	0.694E+00	-11.34	113.6	0.137E+01	-5.42	5.2	W
W	54.00	0.707E+00	-11.18	116.1	0.137E+01	-5.41	-7.4	W
W	56.00	0.758E+00	-10.58	118.1	0.138E+01	-5.40	-20.5	W
W	58.00	0.825E+00	-9.84	119.3	0.138E+01	-5.38	-33.9	W
W	60.00	0.889E+00	-9.19	119.9	0.138E+01	-5.35	-47.6	W
W	62.00	0.940E+00	-8.71	119.9	0.139E+01	-5.32	-61.7	W
W	64.00	0.970E+00	-8.43	119.7	0.139E+01	-5.29	-76.1	W
W	66.00	0.980E+00	-8.34	119.2	0.141E+01	-5.21	-90.1	W
W	68.00	0.971E+00	-8.42	118.6	0.142E+01	-5.11	-104.1	W
W	70.00	0.947E+00	-8.64	117.9	0.144E+01	-5.02	-118.4	W
W	72.00	0.913E+00	-8.96	117.3	0.145E+01	-4.93	-132.8	W
W	74.00	0.873E+00	-9.35	116.6	0.147E+01	-4.83	-147.5	W
W	76.00	0.830E+00	-9.78	115.9	0.148E+01	-4.73	-162.3	W
W	78.00	0.789E+00	-10.22	115.3	0.150E+01	-4.64	-177.3	W
W	80.00	0.751E+00	-10.66	114.8	0.151E+01	-4.56	167.7	W
W	82.00	0.716E+00	-11.06	114.3	0.153E+01	-4.49	152.6	W
W	84.00	0.687E+00	-11.43	114.0	0.154E+01	-4.44	137.5	W
W	86.00	0.663E+00	-11.74	113.7	0.154E+01	-4.39	122.3	W
W	88.00	0.644E+00	-11.99	113.5	0.155E+01	-4.35	107.2	W
W	90.00	0.631E+00	-12.17	113.5	0.156E+01	-4.33	92.0	W
W	92.00	0.622E+00	-12.29	113.5	0.154E+01	-4.39	78.4	W
W	94.00	0.618E+00	-12.34	113.7	0.154E+01	-4.44	64.8	W
W	96.00	0.619E+00	-12.34	114.0	0.153E+01	-4.47	51.2	W
W	98.00	0.623E+00	-12.28	114.3	0.153E+01	-4.48	37.7	W
W	100.00	0.630E+00	-12.18	114.8	0.153E+01	-4.48	24.1	W
W	102.00	0.639E+00	-12.06	115.3	0.153E+01	-4.46	10.7	W
W	104.00	0.649E+00	-11.92	115.9	0.153E+01	-4.46	-2.9	W
W	106.00	0.658E+00	-11.81	116.6	0.154E+01	-4.44	-16.4	W
W	108.00	0.663E+00	-11.74	117.3	0.154E+01	-4.41	-29.8	W
W	110.00	0.663E+00	-11.74	117.9	0.155E+01	-4.37	-43.2	W
W	112.00	0.655E+00	-11.84	118.6	0.156E+01	-4.30	-56.3	W
W	114.00	0.636E+00	-12.09	119.2	0.157E+01	-4.22	-69.4	W
W	116.00	0.606E+00	-12.51	119.7	0.159E+01	-4.12	-82.2	W
W	118.00	0.565E+00	-13.13	119.9	0.162E+01	-3.98	-94.6	W

W	120.00	0.513E+00	-13.96	119.9	0.165E+01	-3.83	-106.8	W
W	122.00	0.457E+00	-14.97	119.3	0.168E+01	-3.67	-118.7	W
W	124.00	0.403E+00	-16.06	118.1	0.171E+01	-3.49	-130.4	W
W	126.00	0.360E+00	-17.04	116.1	0.175E+01	-3.31	-141.9	W
W	128.00	0.339E+00	-17.57	113.6	0.179E+01	-3.13	-153.2	W
W	130.00	0.346E+00	-17.38	111.7	0.183E+01	-2.93	-164.1	W
W	132.00	0.386E+00	-16.43	111.3	0.188E+01	-2.68	-170.1	W
W	134.00	0.456E+00	-14.99	112.4	0.194E+01	-2.43	-176.1	W
W	136.00	0.545E+00	-13.44	114.4	0.199E+01	-2.18	177.7	W
W	138.00	0.637E+00	-12.08	116.8	0.205E+01	-1.93	171.4	W
W	140.00	0.710E+00	-11.14	119.2	0.211E+01	-1.68	165.0	W
W	142.00	0.742E+00	-10.76	121.6	0.217E+01	-1.44	158.4	W
W	144.00	0.721E+00	-11.01	123.7	0.223E+01	-1.20	151.7	W
W	146.00	0.646E+00	-11.96	125.6	0.229E+01	-0.96	145.0	W
W	148.00	0.536E+00	-13.58	126.5	0.236E+01	-0.72	138.2	W
W	150.00	0.427E+00	-15.56	125.1	0.241E+01	-0.51	130.0	W
W	152.00	0.366E+00	-16.90	119.4	0.247E+01	-0.30	121.9	W
W	154.00	0.395E+00	-16.24	112.3	0.253E+01	-0.10	114.1	W
W	156.00	0.526E+00	-13.75	110.1	0.259E+01	0.09	106.6	W
W	158.00	0.734E+00	-10.86	112.6	0.264E+01	0.28	99.5	W
W	160.00	0.967E+00	-8.46	117.4	0.270E+01	0.46	92.7	W
W	162.00	0.116E+01	-6.89	123.7	0.276E+01	0.64	86.3	W
W	164.00	0.125E+01	-6.26	131.9	0.281E+01	0.81	80.3	W
W	166.00	0.121E+01	-6.52	143.7	0.287E+01	0.98	74.6	W
W	168.00	0.109E+01	-7.41	161.2	0.292E+01	1.15	69.4	W
W	170.00	0.100E+01	-8.16	-175.1	0.298E+01	1.31	64.5	W
W	172.00	0.998E+00	-8.18	-151.0	0.303E+01	1.46	60.1	W
W	174.00	0.995E+00	-8.21	-133.6	0.308E+01	1.61	56.1	W
W	176.00	0.853E+00	-9.55	-123.0	0.314E+01	1.76	52.5	W
W	178.00	0.509E+00	-14.04	-117.1	0.319E+01	1.91	49.3	W
W	180.00	0.241E-05	-120.51	-114.8	0.324E+01	2.05	46.5	W

---

* *

****